EXPERIMENTAL AND COMPUTATIONAL INVESTIGATION OF HYDROKINETIC TURBINE

A THESIS SUBMITTED TO
THE GRADUATE SCHOOL OF NATURAL AND APPLIED SCIENCES
OF
MIDDLE EAST TECHNICAL UNIVERSITY

BY

ANIL GÜNEŞ

IN PARTIAL FULFILLMENT OF THE REQUIREMENTS
FOR
THE DEGREE OF MASTER OF SCIENCE
IN
MECHANICAL ENGINEERING

AUGUST 2022

Approval of the thesis:

EXPERIMENTAL AND COMPUTATIONAL INVESTIGATION OF HYDROKINETIC TURBINE

submitted by **ANIL GÜNEŞ** in partial fulfillment of the requirements for the degree of **Master of Science in Mechanical Engineering Department, Middle East Technical University** by,

Prof. Dr. Halil Kalıpçılar
Dean, Graduate School of **Natural and Applied Sciences** _____

Prof. Dr. M. A. Sahir Arıkan
Head of Department, **Mechanical Engineering** _____

Prof. Dr. Mehmet Metin Yavuz
Supervisor, **Mechanical Engineering, METU** _____

Examining Committee Members:

Prof. Dr. Oğuz Uzol
Aerospace Engineering, METU _____

Prof. Dr. Mehmet Metin Yavuz
Mechanical Engineering, METU _____

Assist. Prof. Dr. Özgür Uğraş Baran
Mechanical Engineering, METU _____

Assist. Prof. Dr. Mustafa Perçin
Aerospace Engineering, METU _____

Assist. Prof. Dr. Onur Baş
Mechanical Engineering, TED University _____

Date:

I hereby declare that all information in this document has been obtained and presented in accordance with academic rules and ethical conduct. I also declare that, as required by these rules and conduct, I have fully cited and referenced all material and results that are not original to this work.

Name, Surname: Anıl Güneş

Signature :

ABSTRACT

EXPERIMENTAL AND COMPUTATIONAL INVESTIGATION OF HYDROKINETIC TURBINE

Güneş, Anıl
M.S., Department of Mechanical Engineering
Supervisor: Prof. Dr. Mehmet Metin Yavuz

August 2022, 48 pages

The answer to the increasing amount of energy consumption, mostly in carbon-based energy sources can be found in water and through the wind. The investigation of a special drag-based cross-flow hydrokinetic turbine (referred to as a Vertical Axis Wind Turbine for wind energy applications) called Savonius, is the main purpose of this study. Both experimentally and computationally studying this high self-starting ability turbine will open up the way to small-size energy production with very small water and wind inflow velocities. This study aims to compare the computational results with experimental studies in a water channel, using three different turbine blade base geometries. The semi-circular blade geometry resulted in a good agreement between experimental and computational studies, where both peak around unity tip speed ratio and for maximum power coefficient the relative error is 7.8%. The computational results underestimate the performance compared to experimental result within a margin of 0.03 power coefficient, up to unity tip speed ratio. For $\lambda > 1$ the difference in results of the power coefficient increase up to 1.0. For another base geometry with maximum chamber location near the blade tip, the results of CFD are in close agreement with experimental data for a tip speed ratio interval of $1.1 - 1.7$,

and deviate outside this range.

Keywords: cross-flow hydrokinetic turbine, Savonius, water tunnel experiments, CFD

ÖZ

HİDROKİNETİK TÜRBİNİN DENEYSEL VE BİLGİSAYAR DESTEKLİ HESAPLAMALI İNCELENMESİ

Güneş, Anıl
Yüksek Lisans, Makina Mühendisliği Bölümü
Tez Yöneticisi: Prof. Dr. Mehmet Metin Yavuz

Ağustos 2022 , 48 sayfa

Çoğunlukla karbon bazlı enerji kaynaklarında kaynaklanan, artan miktarda enerji tüketiminin çözümü, su ve rüzgar yoluyla bulunabilir. Savonius adı verilen özel bir sürükleme tabanlı çapraz akışlı hidrokinetik türbinin (rüzgar enerjisi uygulamaları için Dikey Eksenli Rüzgar Türbini olarak anılır) araştırılması bu çalışmanın temel amacıdır. Kendi kendine harekete başlama özelliği gelişkin bu türbini hem deneysel hem de hesaplamalı olarak incelemek, çok küçük su ve rüzgar akış hızları ile küçük boyutlu enerji üretiminin yolunu açacaktır. Bu çalışma, üç farklı türbin kanadı taban geometrisi kullanarak su tünelinde yapılan deneysel çalışmalar yoluyla bilgisayar destekli hesaplamalı sonuçları karşılaştırmayı amaçlamaktadır. Yarım daire şeklindeki kanat geometrisinin, 1 civarındaki kanat ucu hız oranlarında, maksimum güç katsayısı için bağıl hatanın $\%7.8$ olduğu, deneysel ve hesaplamalı çalışmalar kıyaslanması ile sonuçlanmıştır. Hesaplamalı sonuçlar, 1 değerindeki kanat ucu hız oranına kadar güç katsayısında 0.03'lük bir hata payı dahilinde deneysel sonuçla karşılaştırıldığında bilgisayar destekli analiz sonuçlarının performansı saptığını göstermiştir. $\lambda > 1$ için güç katsayısı sonuçlarındaki fark 1.0'a kadar artmaktadır. Azami kalınlık konumuna ka-

nat ucu yakınında sahip başka bir taban geometrisi için, CFD sonuçları, $1.1 - 1.7$ uç hız oranı aralığı için deneysel verilerle yakın bir uyum içindedir ve bu aralığın dışında sapma göstermektedir.

Anahtar Kelimeler: çapraz akışlı hidrokinetik türbin, Savonius, su tüneli deneyleri, CFD

to my mother for who my love always converges to infinity

ACKNOWLEDGMENTS

I would like to express my gratitude to my supervisor Prof. Dr. M. Metin Yavuz for his support of this study, which he started showing during his undergraduate course and continued throughout my Master's program.

I would like to express my gratitude to the examining committee members, Prof. Dr. Oğuz Uzol, Assist. Prof. Dr. Özgür Uğraş Baran, Assist. Prof. Dr. Mustafa Perçin, and Assist. Prof. Dr. Onur Baş for their constructive feedback and valuable suggestions.

I am grateful to have Ertan Karaismail as a mentor, both in the fluid mechanics discipline and in my life. The support of Ahmet Yusuf Gürkan and the NAVIST Engineering Family means the world to me.

I am very thankful to have a friend like Uğurcan Kartal, with whom we started this renewable energy project in our undergraduate years, and friends like Serhat Boztoğan and Huzeyfe Emre Aydın, with whom we worked on this topic with pleasure.

I owe sincere gratitude to my coworker and amazing "Experimental Fluid Mechanics Mind" Oğuzhan Yılmaz. The guidance of Mehmet Özçiftçi during the laboratory work was very valuable.

TABLE OF CONTENTS

LIST OF TABLES

TABLES

LIST OF FIGURES

FIGURES

LIST OF ABBREVIATIONS

2D	2 Dimensional
3D	3 Dimensional
DOF	Degree of Freedom
A_{proj}	Frontal Projection Area of the Turbine
AR	Aspect Ratio
BR	Blockage Ratio
CFD	Computational Fluid Dynamics
CAD	Computer Aided Design
C_f	Skin Friction Coefficient
C_P	Power Coefficient
C_Q	Torque Coefficient
D_T	Diameter of the Turbine
D_{Plate}	Endplate Diameter
D_{shaft}	Shaft Diameter
deg	Degree
EpR	Endplate Ratio
Fr	Froude Number
g	Gravitational Acceleration
H_T	Height of the Turbine
H_{channel}	Height of the Water Channel Section
$\dot{m}$	Mass Flow Rate
L_d	Characteristic Length (Hydraulic Mean Depth)
P_{av}	Available Power
P_{ext}	Extracted Power

PIV	Particle Image Velocimetry
PLA	Polylactic acid
Re_D	Reynolds Number
rpm	Revolution per Minute
SST	Shear Stress Transport
T	Torque
t_{blade}	Blade thickness
U	Inflow Stream Velocity
u_τ	Friction Velocity
y^+	Non-dimensional Distance
VAWT	Vertical Axis Wind Turbine
W_{channel}	Width of the Water Channel Section

Δy	First Layer Thickness
ω	Rotational Velocity
ρ	Density
λ	Tip-speed Ratio
μ	Dynamic Viscosity
ν	Kinematic Viscosity
τ_ω	Wall Shear Stress

CHAPTER 1

INTRODUCTION

The world struggles with the fact that humankind consumes too much energy, mostly in the form of carbon-based non-renewable energy sources, fossil fuels, such as coal and natural gas. To create a counterforce to this enormous momentum of destruction, an important group of scientists, engineers and organizations focused deeply on various aspects of renewable energy. Many engineering disciplines worked together to increase the efficiency of renewables, thus energy extracted from these natural energy sources. While solar energy is the most popular one, its lack of 24-hour operation makes it hard for decision makers to rely on solar PV entirely [6].

The biggest candidates for the noble role of the knight in shining armor to save humankind's future are Wind and Hydropower. The geometric advancement of wind and water turbines made it possible to structure a reliable energy supply to the grid, where each kilowatt-hour of energy extracted from the wind and water source, means burning $500\ gr$ of coil or $210\ dm^3$ of natural gas less [7].

Intuitively, one thinks about two completely different turbine shapes considering wind and hydrokinetic turbines. In megawatt sizes of energy production, a characteristic 3-bladed horizontal axis onshore wind turbine has an average hub height of 80 meters where the rotor diameter can be over 120 meters. On the other hand, a characteristic hydropower plant probably contains a reaction-type turbine (for example Francis or Kaplan type turbines) with a casing including a volute chamber to guide the water flow. The dimension of the turbine diameter can vary from small sizes measured by centimeters to tens of meters, while the blade number is mostly in two digits.

Switching to the other side of the medallion and investigating energy extraction in

watt and kilowatt orders results in a very unique overlap of these two energy types. Considering the rotation axis of a wind turbine, vertical axis wind turbines are the little siblings of horizontal axis wind turbines. Characterizing hydropower turbines as "Reaction versus Impulse" type, cross-flow hydrokinetic turbines (impulse type) take on the role of the little sibling. These two types of turbines, although branched from different family trees, actually are very similar, if not the same, in design and shape. Considering the difference in the working environment of wind and water, these types of turbines can be investigated as a whole in the modern literature. The two types of cross-flow hydrokinetic or vertical axis wind turbines are shown in Figure 1.1.

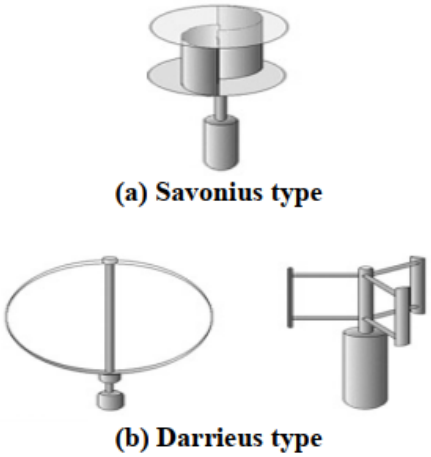

Figure 1.1: (a) Savonius type & (b) Darrieus type turbines. [1]

In many studies, where experimental results are compared with CFD studies or vice versa, only one of these two main processes is performed by the researcher conducting the study. For the other one, a reliable study in this literature field is selected as a validation basis. Although this systematic perfectly generated many successful studies it has some downsides too. Firstly, there is not a consensus on the optimal design of such a drag-based wind/water turbine, because the independent design variables are more than manageable (compared to lift-based turbines). This can cause to skew the result of the study. Secondly, it is an important barrier to future studies where a validation basis case does not exist already. Thus, performing both the experimental and computational parts of such a study can be the key to finding consensus in this research field, considering this present study and many future studies.

In this study, it is tried to take full advantage of the resources the university supplies. It is fortunate enough to have a proper water channel facility and computational resources. Working with both aspects required a clear methodology to achieve the final goals.

The objective of this thesis study is to build the capabilities to conduct experimental and computational studies and compare them to understand the complex dynamics of a Savonius turbine. This objective is fueled by the motivation of verifying that these type of turbines can be used in relatively low speed water and/or wind inflow velocities and small scale off-grid applications.

To create the basis of the study, 3 different blade shapes are selected from literature. Other dimensions of the Savonius turbine, such as the height, are determined considering experimental capabilities. While CFD studies were performed, the model of the turbine is created and printed with additive manufacturing methods. The water channel is re-constructed and characterized. The experimental rig, including a 3D-printed turbine, the shaft, the sensor, and the support holding these types of equipment, is set up inside the water channel test section. Both experimental and computational results are processed and compared. If the results of both studies are consistent, this comparison can be referred to as validation and opens the possibility for future studies.

1.1 Analytical Model

The fundamentals of extracting energy from a free-flowing liquid originate from a basic principle. The fluid flow loses a distinct part of its momentum to a device (turbine) that aims into transform kinetic energy to mechanical energy. This principle is valid whether the fluid of interest is gaseous and the energy extracting device is referred to as a Wind Turbine, or the fluid is liquid, such as water, and the descriptive word changes to “Hydro- “.

The available power of a hydrokinetic cross-flow turbine is calculated by taking the turbine’s area of projection with respect to the flow stream velocity vectors’ surface

normal as the control volume inlet.

$$P_{av} = \frac{1}{2}\dot{m}U^2 \tag{1.1}$$

Where, $\dot{m}$ is the mass flow rate crossing the projection of the turbine and U is the inflow stream velocity.

The mass flow rate can be expressed as;

$$\dot{m} = \rho A_{proj} U \tag{1.2}$$

Where, ρ is the density of the fluid (in this study, water) and A_{proj} is the frontal area, which is simply the product of the diameter (D_T) and height (H_T) of the turbine.

Combining 1.1 and 1.2, the final expression for the available power can be shown as;

$$P_{av} = \frac{1}{2}\rho A_{proj} U^3 \tag{1.3}$$

Note that all of the variables at the RHS of the equation are either known or can be controlled in wind or water channels. The inflow stream velocity causes a force, which can create torque for a proper turbine blade shape. Thus the extracted power can be calculated as such,

$$P_{ext} = T \times \omega \tag{1.4}$$

Where, T is the torque and ω is the angular velocity of the turbine.

Equations 1.3 and 1.4 combined, where the extracted power is divided by the available power, results in one of the most important performance parameters of turbine technology: The Power Coefficient [1.5]. This coefficient, by its definition, is actually an efficiency for the turbine and is limited by the famous Betz number (Betz # = 16/27 = 59.26).

$$C_P = \frac{P_{ext}}{P_{av}} = \frac{T \times \omega}{\frac{1}{2}\rho A_{proj} U^3} \tag{1.5}$$

While the power coefficient is crucial as an output parameter, a proper variable should be selected to compare the performance of turbines. An important consensus of the turbine technology literature indicates that the performance curves are data of power coefficient versus tip-speed ratio.

Mathematically expressed,

$$\lambda = \frac{\omega \times (D_T/2)}{U} \tag{1.6}$$

Where, D_T is the diameter of the turbine.

While the most important equations are already presented, it could be useful to define other geometric and output parameters too.

A unique design parameter for cross-flow turbines takes the fraction between width and height into account. The Aspect Ratio can be defined as,

$$AR = \frac{H_T}{D_T} \tag{1.7}$$

An important part of the design and the 2D assumption is the usage of endplates, where the Endplate Ratio can be calculated as,

$$EpR = \frac{D_{\text{Plate}}}{D_T} \tag{1.8}$$

The physical presence of the turbine inside a finite area channel, water channel test section, creates a disturbance which can be corrected knowing the Blockage Ratio, expressed as,

$$BR = \frac{H_T D_T}{H_{\text{channel}}\, W_{\text{channel}}} \tag{1.9}$$

Where, H_{channel} and W_{channel} are the height and width of the water channel section, respectively.

While the power coefficient gives a good understanding of the rated performance, another output parameter should be defined to represent the starting ability. The Torque Coefficient is mathematically expressed as,

$$C_Q = \frac{4T}{\rho H_T D_T^2 U^2} \tag{1.10}$$

Noting that this expression can be used for both static and dynamic torque coefficient calculations.

To understand the flow regime of an open channel flow, Froude Number is intoduced as,

$$Fr = \frac{U}{\sqrt{gL_d}} \tag{1.11}$$

Where, g is the gravitational acceleration and L_d is the characteristic length that represents hydraulic mean depth in open channel flow.

1.2 Literature Review

The literature review can be divided into four main parts. Firstly, the fundamentals of hydropower are laid out to understand the order of magnitude. Afterward, the concept of cross-flow hydrokinetic turbines is introduced, where Savonius and Darrieus type turbines are explained and compared. The next part explains and compares wind and hydro turbines, pointing out major similarities that help understand the topic further. The final and most important part contains the literature about Savonius turbines, in which hydrokinetic turbine technology is supported with wind energy applications.

According to the 2022 Hydropower Status Report, published by the centralized organization, International Hydropower Association, the installed hydropower capacity reached 1360 GW with an annual growth of 1.9% [8]. While China leads this market with nearly 400 GW installed capacity, Brazil and the USA rank second and third, with just over 100 GW. Turkey, with 31.5 GW, is the second most hydropower installed European country just after Norway, with 33.4 GW. At this point, the energy production is divided into two parts, where the majority of these GWs are extracted by traditional/conventional hydrokinetic turbines, such as propeller turbines (Kaplan) and Francis turbines [9]. The winner of the trade-off between higher energy production and high initial cost and effort was obvious. Noting that this initial effort was civil work dominated and had a huge impact on carbon and greenhouse gas emissions, the very phenomena these types of energy sources aim to stop [10]. But with the cumulatively increasing adverse effects, such as damages to aquatic life and deterioration of water quality, summarized by Sood and Singal [11], the renewable energy world shifted its focus to non-traditional or unconventional methods. These small-scale hydropower applications created a win-win situation because while minimizing the adverse effects, they opened up the possibility for very small head and/or velocity energy production. Quaranta [12], represents an excellent solution path for the already existing hydraulic infrastructures towards “Very Low Head” energy production. However, for new projects, cross-flow type turbines could be the answer to many

challenges, with minimal harm to aquatic life, very low initial cost, and the ability to unlock small-scale hydro potential [2].

Narrowing down the complete hydropower spectrum to cross-flow turbines means investigating the two vertical axis type turbines, Savonius and Darrieus. The main difference between the Savonius and Darrieus type turbines is the driving force, which creates rotating motion. While Darrieus turbines are airfoil shaped and are referred to as "lift-based", Savonius turbines as classified as "drag-based" turbines. Akwa et al. [13] compared different types of wind turbines according to their average performance coefficients versus tip speed ratio. Figure 1.2 shows how superior other types of turbines, including Darrieus, are against Savonius when power coefficient is the output metric. At this point, the most crucial conclusion can be that, while vertical axis turbines are not substitutes to megawatt producing conventional horizontal axis turbines, the real comparison is between the Darrieus and Savonius. The game-changing advantage of Savonius over Darrieus is its high torque coefficient, which is achievable in low tip speed velocities. The need for high tip speed ratios, i.e. higher inflow velocities, makes it impractical for Darrieus rotors to compete with the drag-based Savonius turbine in low head and/or small inflow velocity applications.

Saini and Saini [14] studied the hybrid turbine setup by combining a two-bladed Savonius turbine core with a three-bladed Darrieus turbine around it. The results pointed out that both the advantages of Savonius type turbines (a good self-starting ability) and Darrieus type turbines (a high maximum power coefficient) can be achieved in the hybrid model. Jahangir Alam and Iqbal [1] studied the similar problem with a slightly different geometry and concluded that for very low inflow velocities, below 1 m/s rated water flow, the Savonius turbine alone resulted in a larger power coefficient than the hybrid model.

What makes these vertical axis turbines special is that they can be used both as wind- and hydro-turbines. This intersection point opens up the possibility for researchers to harvest the literature in both areas. The main difference lies in the density of the actuator fluids and results in similar performance values for the same inflow velocity. Bahaj and Myers [15] predicted that, for the same swept area, the torque for a hydrokinetic turbine is roundly 4 times the torque produced by a wind turbine rated

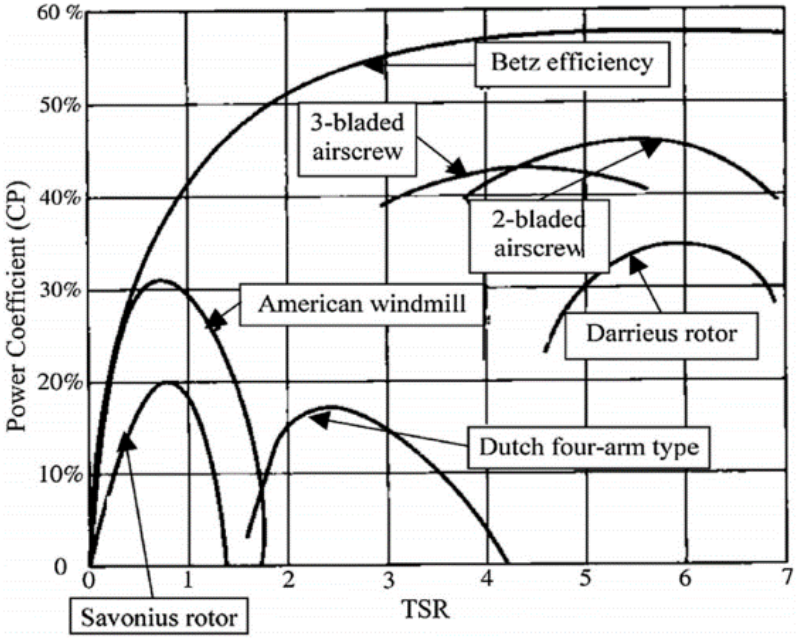

Figure 1.2: Typical power coefficient performance curves as a function of tip speed ratio for various turbine types [2]

at 2-3 m/s inflow velocity. The study conducted by Zhang et al. [3], compared drag-based rotor originated from a Savonius turbine. Since the power coefficient trend is similar for water and wind originated turbines, the results of this study, shown in Figure 1.3, give a clear understanding on the trends of the performance curve.

Although the usage of Savonius turbines become popular in the last two decades, the idea is nearly a century old. The name father Sigurd Johannes Savonius, a Finnish inventor, patented his idea of a "Rotor Adapted to be Driven by Wind and Flowing Water" in 1925 [16]. Since this first two-bladed design many researchers worked to improve performance originating on one simple fact: increasing the positive (desired rotation direction) torque and/or decreasing the negative torque created by the inflow to maximize the net torque on the turbine. The investigation topics were mostly about the blade numbers, blade shapes, positioning of the blades relative to each other, 3D twist angle, end plates, and usage of obstacles.

Unfortunately, there is not any consensus about some crucial design parameters. For example, while Saad et al. [17] argue that the overlap ratio for torque maximization

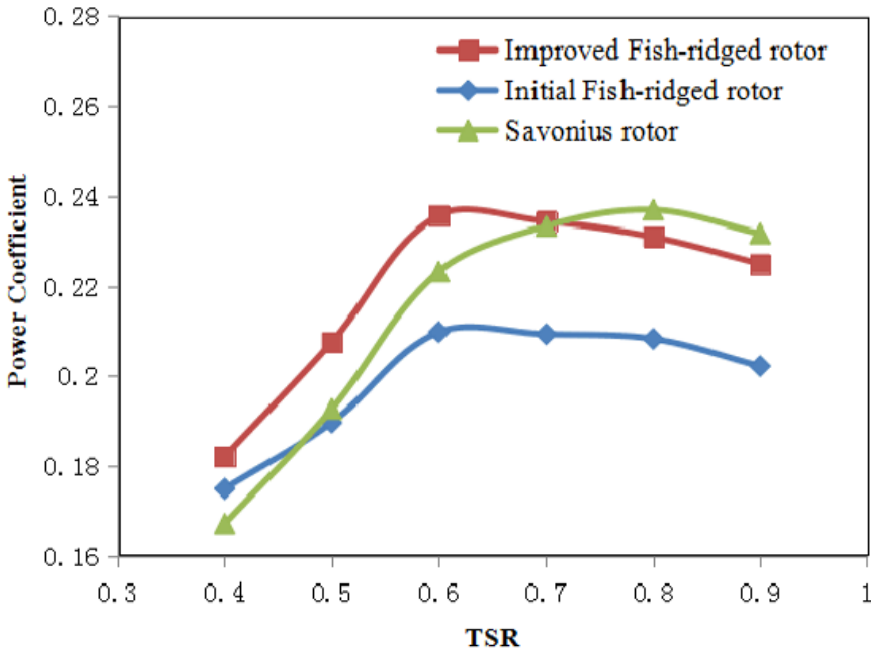

Figure 1.3: Characteristic power coefficient versus tip speed ratio graphs for various wind turbine types [3]

is 0, the studies of Damak et al. [18] pointed to a non-zero overlap ratio between 20 and 30 %. The overlap creates a gap between blades where in some angular positions flow can escape without creating negative torque. Obviously, this leads to a huge advantage but also tweaks the discussion about the blade numbers. Ross and Altman's study [19] clearly shows that having a two-bladed Savonius with overlap has the above-explained advantage, but otherwise having a three-blade drag-based turbine with overlap makes the gap practically redundant since in only few, if any, angular positions the gap acts as a negative torque relief. This is the reason why many studies of blade numbers, obtain the higher performance with two blades [20, 21, 22].

The twist angle is the major factor that makes the flow three-dimensional, thus affecting the performance. While twisting the blades in the direction of height up to a certain angle increases the power coefficient, beyond an angle the upstream flow became disturbed and the effect is reversed. Both Saad et al. [17] and El-Askary et al. [23] came to the conclusion that a 45° helix angle is optimal for Savonius type turbines.

The blade shape discussion in the literature is still a hot topic, where different funda-

mental ideas are discussed and many outcomes are made. Tartuferi et al. [24] studied a unique design where the drag-based categorized Savonius turbine blades evolve into high-chambered airfoil shapes of SR3345 and SR5050. This particular shape, with the trait of a chamber, took advantage of the low-pressure region on the rear end of the advancing blade and increased the performance. Liskiewicz et al. [4] studied three different blade shapes, starting with classical semi-circular Savonius blades, and mainly investigated a special spline-shaped blade with three characteristic points as shown in Figure 1.4. Saha et al. [5] worked on a hydrokinetic turbine with a shape derived from an ellipse, presented in Figure 1.5.

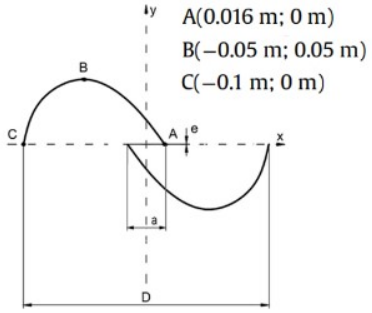

Figure 1.4: Special spline shaped blade with three characteristic points, A, B & C. [4]

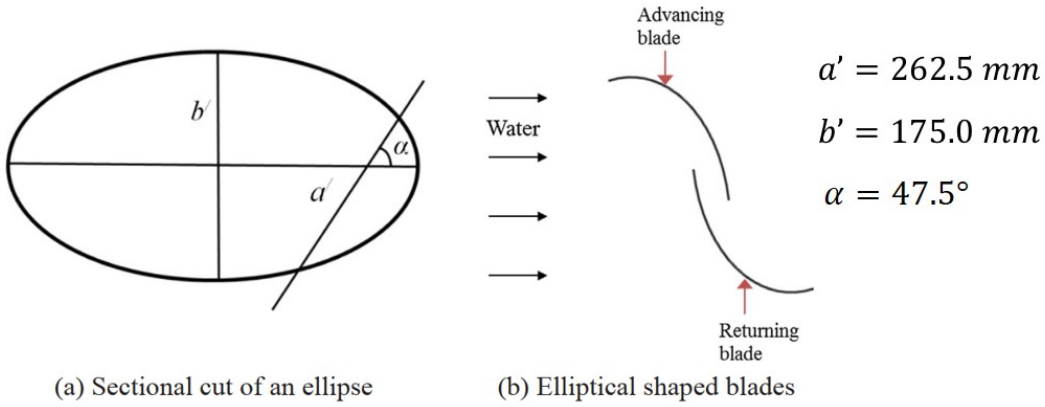

Figure 1.5: Spline shaped blade derived from an ellipse.[5]

The usage of end plates in drag-based vertical axis turbines is one of the most cost-effective and easy ways to increase performance. While researchers studied the optimal end plate diameter and found similar but slightly different values, Saha et al. [5] pointed to the most convenient choice, 1.1 times the Savonius turbine diameter.

The fact that end plates assure the pressure contours are uninterrupted throughout the height (mainly at the upper and lower ends) between the concave and convex sides of the blade, makes them an important design part for two-dimensional studies.

The aspect ratio of a cross-flow turbine explained in Equation 1.7, is investigated by many researchers, and two important outcomes about maximum and minimum values are made. Prabhu et al. [25] studied hydrokinetic turbines and concluded that after a 1.8 aspect ratio the power coefficient values reach a plateau. The study of Saha et al. [5] on the other hand defined the practical minimum for a two-dimensional study, where an aspect ratio equal or greater to unity adequately predicts the flow physics.

Obstacles that guide or block the flow can be used to increase the net torque value. Thiyagaraj et al. [26] studied a different kind of obstacles including single and double deflector plates, guide boxes, and nozzles and noted the performance increase.

Birjandi et al. [27] investigated the power output of hydrokinetic turbine considering the free surface and blockage ratio effect. The test section is 61 cm in width and in full condition filled with 60 cm in water height, where the maximum pump operation condition results in a 1 m/s inflow velocity. A clearance coefficient is defined as the fraction of the water height above the turbine and the turbine diameter is defined. Different type of turbines and their typical clearance coefficient ranges are given. Experiments performed with a Darrieus type turbine inside the explained water channel test section, with positive (fully submerged turbine), negative (partially submerged turbine, which experienced a two-phase phenomenon), and approximately zero clearance coefficient, pointed out the result that the maximum power coefficient can be archived beyond Betz's limit with a partially submerged turbine. It can be understood that a fully submerged turbine with a roundly 0.5 clearance coefficient is safe to work on considering the water inflow range of this study.

Lartiga and Crawford [28] worked on water channel blockage ratio effects with PIV as a high accuracy post-processing tool. The study compared the theory with 5.5%, 9%, 20%, and 55% blockage ratios inside a water domain. For trust coefficient values less than 0.5 the power coefficient results were nearly identical and the main deviation occurred at the very end of the trust coefficient range of 0.9 – 1.0, wherein the power coefficient decreases in theory but contrarily in practice increases further with block-

age ratio. While for 55% blockage the results deviate crucially, smaller blockage ratio values only differ slightly. For example, the maximum corrected (equivalent) inflow velocity is just below 1.05 and 1.10, of the original inflow velocity for 5.5% and 20% blockage, respectively. This study shows that while a 55% blockage deviates the results dramatically, a blockage ratio below 20% minimally effects the results obtained in a water channel.

In the effort of CFD model validation, Saad et al. [17] excellently compares four mostly used turbulence models: Standard k-ε, Realizable k-ε, RNG k-ε, and SST k-ω. This study uses Fujisawa's [29] experiments as a basis, where the Savonius turbine diameter is 30 cm and zero-overlap configuration is also tested (very similar to the current study). Saad et al. tabulated the correlation coefficient, explained by Tahani et al. [30], varying from zero to one, where unity means perfect correlation. While Standard and RNG k-ε models were below 0.8, and the best k-ε model is Realizable with 0.885, the best turbulence model stands out with 0.943 as SST k-ω. While Fujisawa had a +-5% uncertainty in the experiments, the SST k-ω results were in good agreement with a maximum of 4.3% deviation in static torque coefficient. Tahani et al. point out the fact that k-ε models as not sufficient in capturing vortex regions, while SST models can be trusted for this phenomenon. The cost, in computational power and time, is the small y+ value. To capture the flow physics, especially the boundary layer with high-velocity gradient, this non-dimensional distance should be below unity.

1.3 Outline of the Thesis Study

In Chapter 2, the effort of experimental studies is presented. Starting from the water channel and the design of the Savonius turbine, experimental setup and measurement techniques are explained. In Chapter 3, computational fluid dynamics studies are presented. The results of the experimental and computational chapters are presented and compared in Chapter 4. Finally, in Chapter 5, discussions and conclusions are made to finalize the thesis study.

CHAPTER 2

EXPERIMENTAL SET-UP AND MEASUREMENT TECHNIQUES

2.1 Reconstruction and Calibration of Water Channel

The water channel is located in the Middle East Technical University - Mechanical Engineering Department's Graduate Fluid Laboratory, in Ankara/TURKEY. This channel was built in 2013 and hosted a similar kind of study, where a Darrieus type cross-flow hydrokinetic turbine is investigated [31]. The whole set-up mainly consists of, a tank (upstream reservoir) followed by a flow straightener system, a contraction section and test section, a tank (downstream reservoir), and two parallel and symmetric 12" pipelines that return the flow with the help of axial pumps.

The parallel pumps are supplied by a national pump manufacturer, HCP PUMP Systems, classified as "High-capacity Freshwater and Seawater Pumps". The axial flow model L-300A, with a bronze propeller and 420 m^3/h rated flowrate, is used. Although the rated rotational velocity of a pump is cataloged as 1500 rpm, the system can only achieve 1473 rpm as the rated maximum.

The test section of transparent plexiglass is 6.0 m in length, and 0.8 m in width. The test section can be filled with water up to 0.95 meters. Between [4.5 m – 5.0 m] of the test section a structural support has been constructed to hold the necessary equipment. This is the place where the shaft is constrained in transverse motion with a ball bearing and the Savonius turbine is placed. A "GAMAK AGM 71 4a" motor is used the drive the turbine at constant rotational velocity.

In the scope of re-constructing the water channel two main steps were taken. Firstly, the two pumps are disassembled and the insides are cleaned and coated for further

protection. Secondly, a new honeycomb and flow screen system is assembled to the upstream of the test section. The hexagon structure of the honeycomb mesh has a side-to-side length of 8.6 mm, where the wire screen square mesh size is 1 mm.

Figure 2.1: A photograph of the water channel

Figure 2.2: A photograph of one of the HPC L-300A Pumps

In the current study, calibration of the water channel means knowing the velocity of the water considering two independent variables: the height of the water inside the test section (H_{channel}) and the operation velocity of the HPC L-300A Pump System. Changing H_{channel} from 55 cm to 70 cm with 5 cm increments and varying the rota-

tional velocity from 0 to 1473 rpm, measurements were taken.

The measurements aim to determine the velocity in the longitudinal direction of the 6-meters-long test section. A buoy system, which contains one floating and one sinking component is used, so that a smooth floating inside the water is achieved. Since the frontal surface area of the buoy system is minimal compared to the water channel test section area, it can be used for the calibration of the water channel. After filling the water channel to the predetermined test section height (first independent variable of the calibration) and adjusting the pump system rotational velocity (second independent variable), the buoy system is placed in the upstream tank and the time of travel to the downstream tank, through the 6-meters-long test section is recorded. Using the simple distance-speed-time formulation the water channel velocity values are calculated and presented in Figure 2.3.

The water channel test section can hold up a water height of 0.95 m before spilling but having H_{channel} values greater than 0.7 m is impractical for safety reasons. The transient phases of the pump system operation cause a highly waved potential towards the downstream tank and can result in an outpour of a large amount of water.

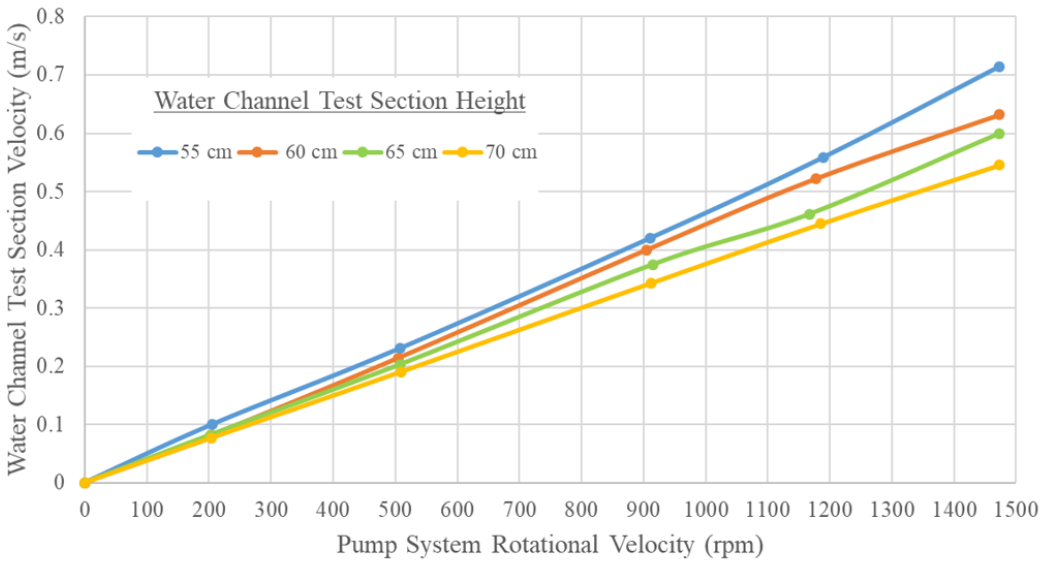

Figure 2.3: Calibration of the Water channel Test Section Velocity by, plotting water channel test section velocity versus pump system rotational velocity, for four discrete water channel test section heights.

2.2 Savonius Hydrokinetic Turbine inside the Water Channel

2.2.1 Shape of the Savonius Turbine Blades

The most important part of this study is the shape of the turbine blades. Since only two-dimensional effects are investigated, all design parameters affecting the performance of a Savonius turbine can be reduced to the 2D profile normal to the direction of height. Many studies use a classical semi-circular Savonius blade profile as the base geometry. In this study, a second and third basis geometry is selected and investigated both experimentally and computationally. As explained in the Literature Review, Liskiewicz et al. [4] suggested a special spline shape with 3 characteristic points and Saha et al. [5] worked on an elliptical shape. All three basis geometries are shown in Figure 2.4, where turbine diameter, D_T, shaft diameter, D_{shaft} and blade thickness, t_{blade}, are kept constant.

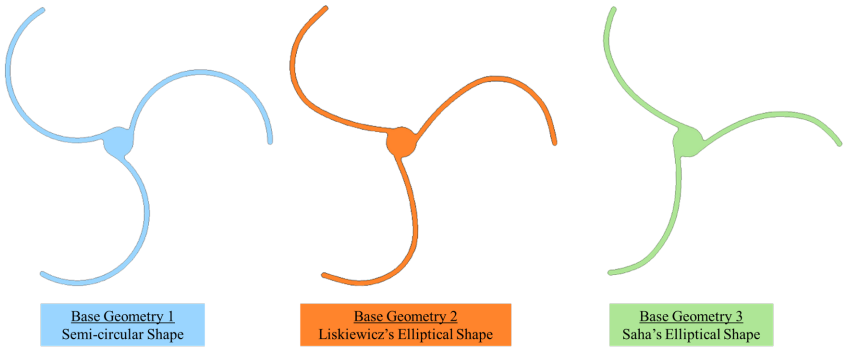

Figure 2.4: The 3 Base Geometries selected for experimental investigation

2.2.2 The Design of the Savonius Turbine

As explained in the Literature Review, an aspect ratio of unity can accurately predict the flow physics in two-dimensional studies [5], thus AR=1 is selected.

The determination of the dimensions of the Savonius turbine is an iterative process. This process is aimed to shorten the knowledge gained from the literature (e.g. selecting aspect ratio as unity). For the first iteration, having a test section water height, H_{channel}, of $0.60\ m$ is a logical choice considering the subchapter where calibration

is explained. Since W_{channel}=0.8 m, a fixed variable in the test section is known. According to Equation 1.9 the blockage ratio is defined by the turbine dimensions since the denominator is a constant. While decreasing the blockage ratio makes the experimental results more accurate, it also reduces the turbine dimensions too much for an adequate study. Selecting a 20% blockage ratio results in a sweet spot where blockage effects are minimized [28] and Savonius turbine dimensions are significant enough. Solving the blockage ratio equation results in $D_T = H_T \approx 0.31\ m$. If the $0.31\ m \times 0.31\ m$, Savonius turbine is placed in the geometric center of the $0.60\ m \times 0.80\ m$ test section the clearance coefficient (fraction of the water height above the turbine and the turbine diameter) is not greater than 0.5. The free surface drop just behind the turbine can be crucial and could influence the results. Thus a second iteration is made where turbine design parameters (including the location of the Savonius turbine inside the test section) are unchanged and only the water height increases by $5\ cm$. This results in $0.31\ m \times 0.31\ m$ turbine inside a $0.65\ m \times 0.80\ m$ test section with clearance coefficient greater than 0.6 and $BR \approx 18.5\%$.

For $0.4\ m/s$ water channel velocity, the water channel test section height of $0.65\ m$ results in a Froude Number of roundly 0.158 using Equation 1.11. Noting that this result is less than unity, where $Fr = 1.0$ defines a critical flow with critical mean depth versus critical velocity. For $0.4\ m/s$ water channel velocity, the critical depth can be calculated as $1.6\ cm$. Since, $0.158 < 1.0$, or $65\ cm > 1.6\ cm$, the inertia forces of the water tunnel test section flow are not dominant and the waves minimally disturb the experimental data collected. Also, comparing the order of viscous forces with inertial forces, the boundary layer thickness at the test section can be calculated as $1.2\ cm$ and can be assumed to have a negligible influence on the acquired data.

To have good structural integrity, the blade thickness is selected as t_{blade}=5 mm. This value is also the thickness of the hollow part where a shaft is assembled to transfer the movement. The shaft diameter is selected as D_{shaft}=20 mm, so that there is an interference fit between the shaft and the ball bearing of the same internal diameter.

A 3-bladed Savonius turbine can be easily divided into three equal parts of 120° (including the hollow midsection covering the shaft) and its continuous geometry throughout the height makes it very easy to manufacture by 3D printing. Considering

strength properties and the work environment of water, PLA is selected as the additive material. The 3D-printed parts are bonded together with a special glue for PLA. The blades and the shaft have M4 holes aligned to each other so that the assembly can transfer the torque without a slip and loss.

The design of the Savonius turbine is summarized in Table 2.1 and illustrated in Figure 2.5. The assembly of the test section is given as Figure 2.6, where all important components are labeled. The water channel test section, filled with water is presented in Figure 2.7.

Table 2.1: Details of Savonius Turbine Design Parameters

Parameter	**Value/Feature**
D_T	0.31 m
H_T	0.31 m
Aspect Ratio, AR	1 (unity)
Blockage Ratio, BR	18.5%
Clearance Coefficient	0.63
D_{shaft}	20 mm
t_{blade}	5 mm
Material	PLA
Blade Number	3

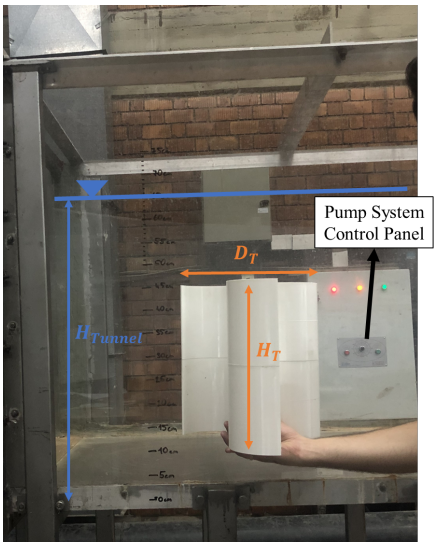

Figure 2.5: Base Geometry 1 Savonius turbine

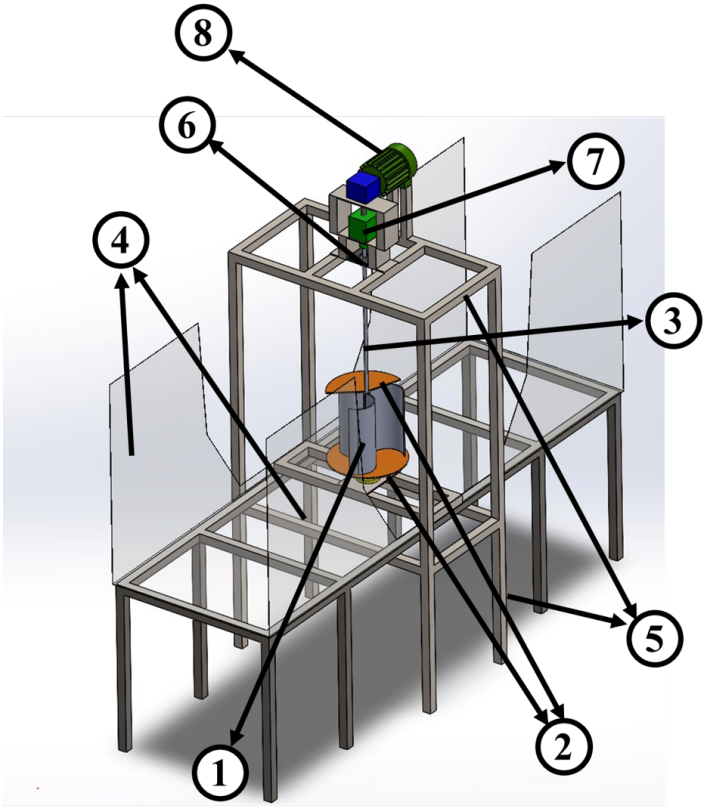

(1) Savonius turbine (2) End plates (3) Shaft
(4) Water tunnel test section side plexiglass
(5) Support system (6) Ball bearing
(7) Sensor (8) Motor

Figure 2.6: Assembly of the test section

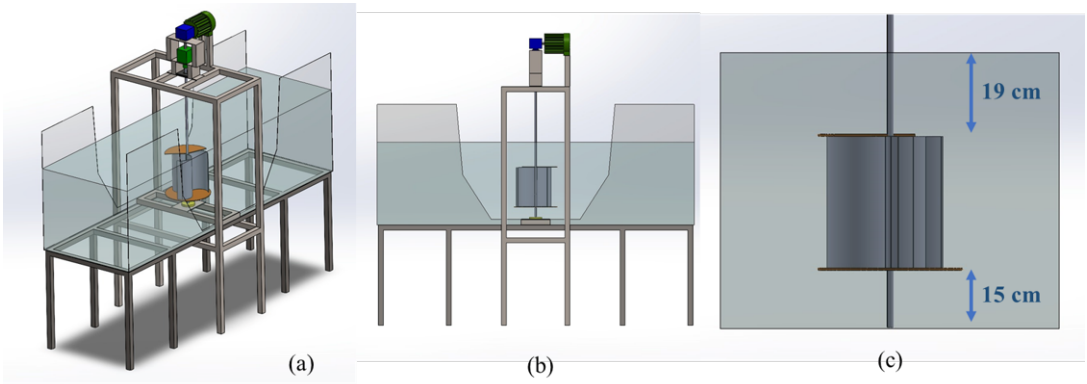

Figure 2.7: (a) Isometric view (b) Side view of the test section (c) Savonius Turbine location inside the fluid volume

2.3 Sensor and Measurement

2.3.1 The Torque and RPM Sensor

Labeled, as (7), in Figure 2.6 a Burster 8661 torque sensor is used to measure both static and dynamic torque values along with rotational speed or angular displacement. Coupled with easy-to-use software, DigiVision, the 8661-5010 Model available in the laboratory, is equipped with an integral speed/angle measurement encoder disk with 400 increments (maximum resolution of 0.225°, i.e. maximum speed measurement of 15.000 rpm) and has a +-0.1% F.S. tolerance of sensitivity. The torque measurement range for this sensor is +-10N.m, which ensures a safe experimental procedure regarding the dynamic overload safe.

The Burster 8661 torque sensor contains a total of four strain gauges arranged onside the torsion shaft as a Wheatstone-bridge circuit. There is a linear relationship between the torque applied and the output voltage of the circuit. With the aim of having a higher accuracy, the output voltage is amplified before digitized and monitored in the DigiVision Software. Catalog images and design principles of the sensor are presented in Figure 2.8.

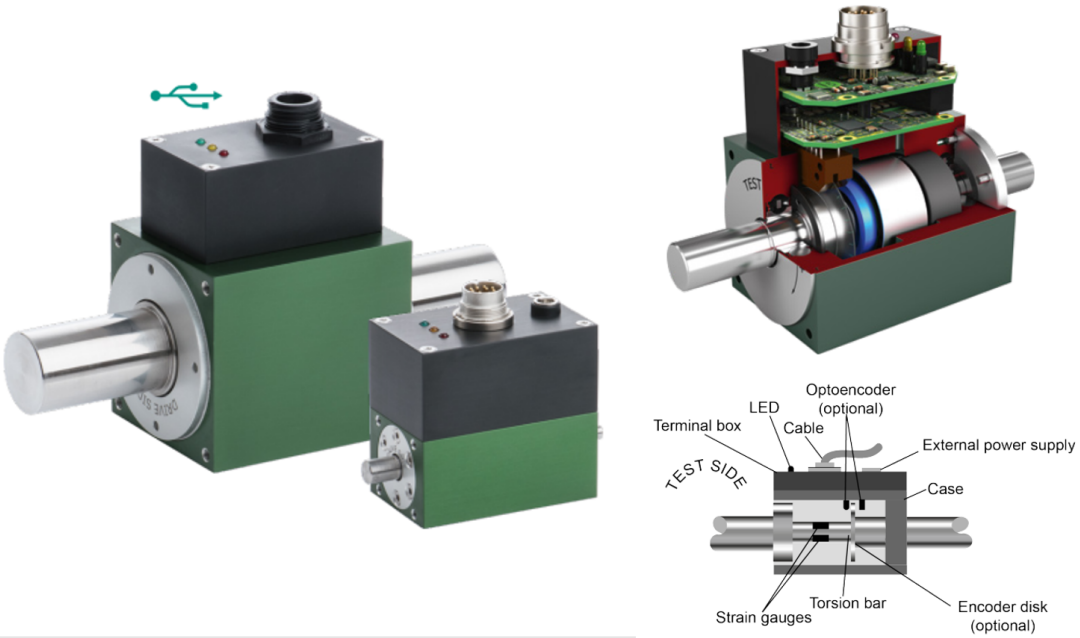

Figure 2.8: Catalog images and design principle of the Burster 8661 torque sensor

2.3.2 Measurement Procedure

Figure 2.3 shows a monotonic increase in inflow velocity with increasing pump rotational speed, for a constant water channel test section height. It is impractical to simulate these transient inflow conditions in further steps of this study. Thus, the data acquisition process of the experimental study starts after the pump is operated for at least 5 minutes so that all transient effects are minimized. At the moment the turbine is set to be free to rotate, the data is recorded. The data is interpreted, formalized, and visualized via MS Excel, which is the primary digitized output of the measurement device.

Focusing on the $0.65\ m$ water channel test section height curve in Figure 2.3, at $1000\ rpm$ pump system rotational velocity the channel velocity is equivalent to $0.40\ m/s$. The pump system control panel labeled in Figure 2.5 is adjusted to this rotational velocity value. For each of the three base geometries, experiments are performed for $0.40\ m/s$ inflow velocity. The motor, labeled as (8) in Figure 2.6, drives the turbine shaft up to $60\ rpm$ rotational velocity with increments of $6\ rpm$. Using Equation 1.6 to calculate the tip speed ratio for the inflow velocity and changing rotational velocity, a tip speed ratio range of $0 - 2.42$ can be investigated.

For a constant inflow velocity (i.e. the denominator of tip speed ratio is constant, Equation 1.6) and controlled turbine rotational velocity values torque results are investigated. This torque value contains both inertial and hydrokinetic components. Thus the inertial torque values are also pre-recorded and extracted from these results.

CHAPTER 3

COMPUTATIONAL FLUID DYNAMICS (CFD) STUDIES

3.1 CFD Software Programs

In this study, a commercially available package system, ANSYS, is used, which divides the pre-processing step into three subparts: "CAD-Geometry and Domain Creation", "Meshing – Creating the Mesh Structure", and "Setting up FLUENT Solver". While for the CAD part SpaceClaim Direct Modeler is used, the mesh is created with the ANSYS Mesher tool. ANSYS – Fluent solver is used for the solving process.

3.2 CAD - Geometry and Domain Creation

These types of studies designate the dimensions with respect to the main component's dimension. In this case, this basis is the diameter of the 2D Savonius turbine. As shown in Figure 3.1 the inner domain size is twice in diameter of the turbine. Figure 3.2 shows the upstream, downstream, and side wall distances as a function of turbine diameter. Noting that this outer domain results in the water channel dimensions to ease the comparison between experimental and computational results.

3.3 Meshing – Creating the Mesh Structure

As explained in the Literature Review section y^+ is a crucial non-dimensional parameter for distance, i.e. size of the mesh inside the boundary layer. y^+ is directly proportional to the "First Layer Thickness" (a direct input for any meshing software,

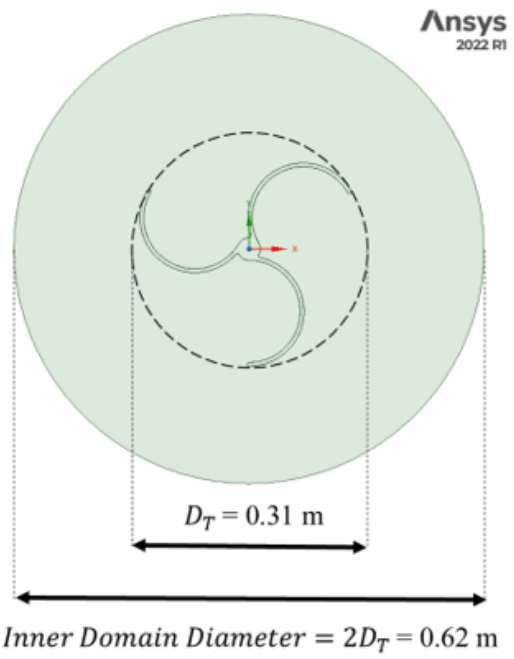

Figure 3.1: Details of the inner fluid domain

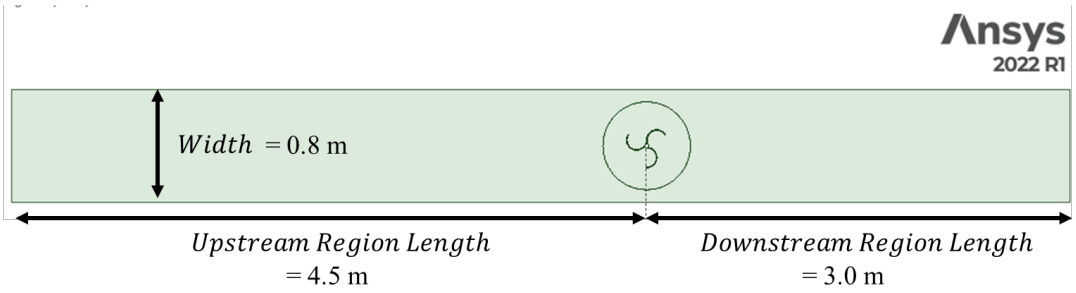

Figure 3.2: Details of the outer fluid domain

thus very important to determine) and can be expressed mathematically as,

$$y^+ = \frac{\Delta y \cdot u_\tau \cdot \rho}{\mu} \tag{3.1}$$

Where, Δy is the first layer thickness $[\mathrm{m}]$, u_T is the friction velocity $[\mathrm{m/s}]$, ρ is density $[\mathrm{kg/m3}]$, μ is the dynamic viscosity [$\mathrm{Ns/m2}$], and ν is the kinematic viscosity [m2/s].

The friction velocity can be expressed as,

$$u_T = \sqrt{\frac{\tau_\omega}{\rho}} \tag{3.2}$$

Where, τ_ω is the wall shear stress and can be further represented as,

$$\tau_\omega = \frac{1}{2} C_f \rho U^2 \tag{3.3}$$

Where, U is the free inflow velocity and C_f is a non-dimensional number called skin friction coefficient which can be associated with another non-dimensional flow property as,

$$C_f = 0,0576 \left(\mathrm{Re}_x\right)^{-0,2} \tag{3.4}$$

Where, Re_x represents the Reynold Number based on the turbine diameter $D_{T'}$,

$$Re_x = Re_D = \frac{\rho U D_T}{\mu} \tag{3.5}$$

From the water channel calibration study, take V_1=U=0,4 m/s.

Since the y^+ values is aimed to be less than unity, assume $y^+ = 1$, so that every variable except the aim to find (Δy) is the only unknown. Table 3.1 summarizes this analytic process to find "First Layer Thickness".

Table 3.1: Calculation of First Layer Thickness

Variable	**Value**	**Dimension**
Free inflow velocity, U	0,5	m/s
Savonius turbine diameter, D_T	0,31	m/s
Water density, ρ	997	kg/m3
Dynamic viscosity, μ	0,000891	Pa s
Kinematic viscosity, ν	8,93565E-07	m2/s
Reynolds Number, Re_D (Eqn. 3.5)	173000	-
Skin friction coefficient, C_f (Eqn. 3.4)	0,00516	-
Wall shear stress, τ_ω (Eqn. 3.3	0,643	Pa
Friction velocity, u_T (Eqn. 3.2	0,0254	m/s
Non-dimensional distance, y^+ (assumed)	1	-
First Layer Thickness (Eqn. 3.1)	0,000035187	m
	0,035187	mm

It is usual that the tip speed ratio exceeds unity in Savonius type turbines. Thus it would be safe to use a safety factor of 2 considering the first layer thickness and use $\Delta y = 0.017mm$.

Figures 3.3 and 3.4 present details of the mesh structures, the inflation layers and the relation between moving, and stationary domains. Figure 3.5 shows the sphere of influence option applied to downstream of the outer domain mesh structure to ensure a smooth mesh transition.

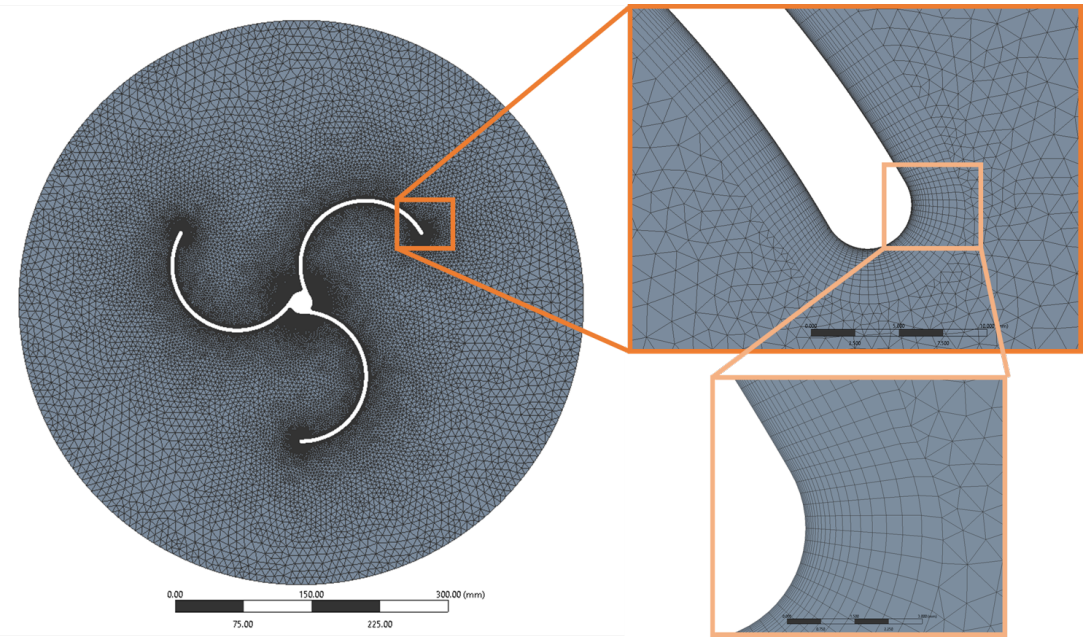

Figure 3.3: Details of inner domain mesh structure including the tip of the Savonius turbine and the inflation structure

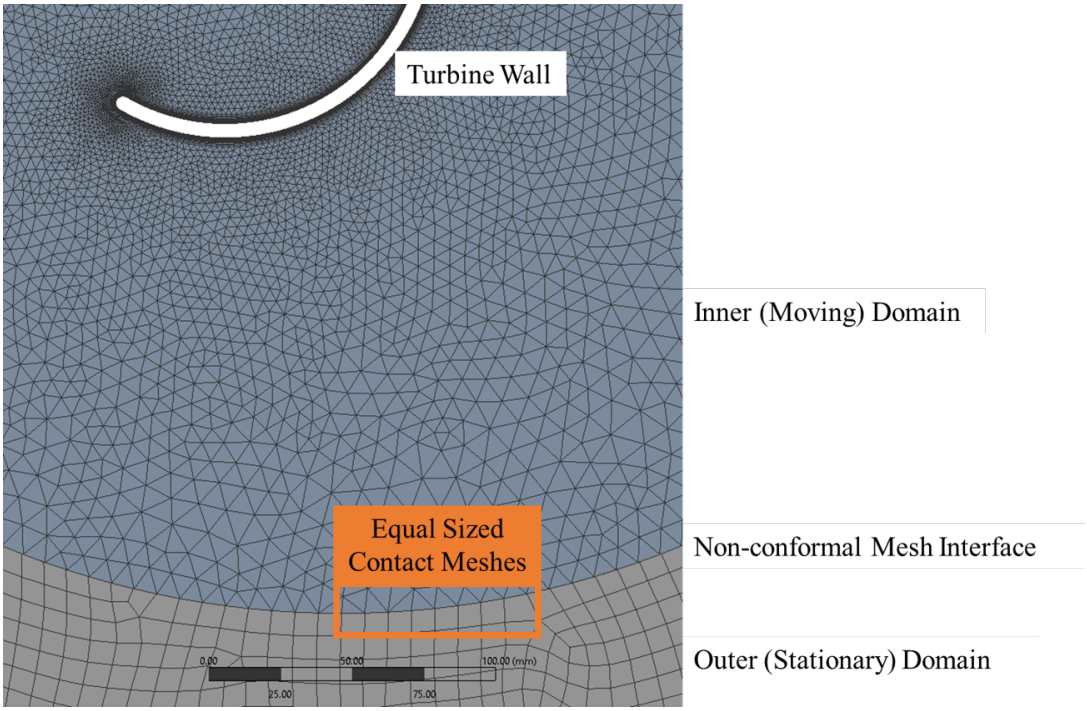

Figure 3.4: Relation between the inner and outer domain mesh structures

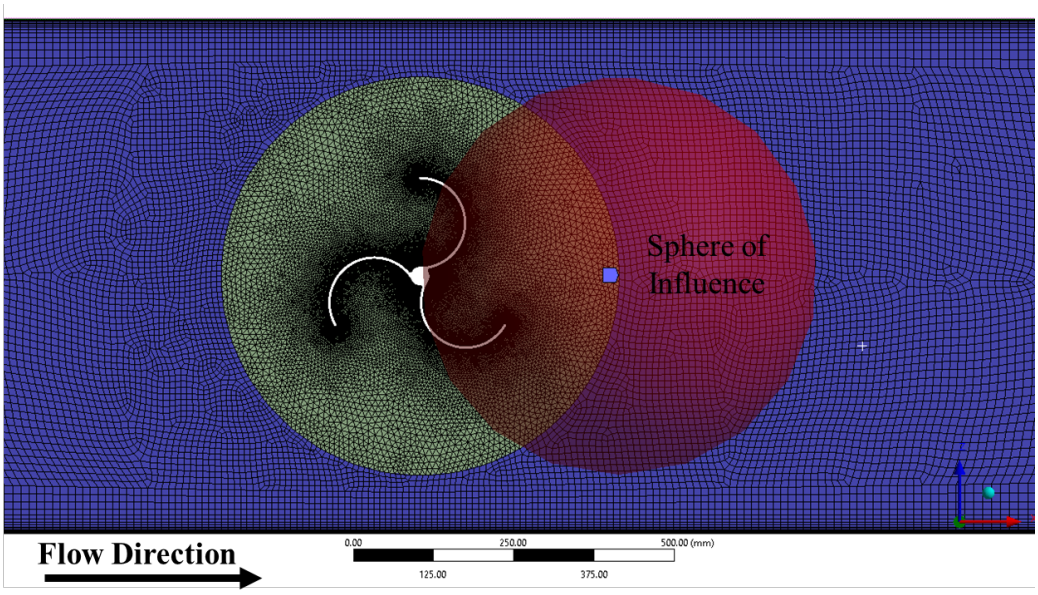

Figure 3.5: The sphere of influence option applied to the downstream of the outer domain mesh structure

3.4 Solver – Setting up FLUENT Solver

The analysis type is “Pressure-Based”, the velocity formulation “Absolute”, the 2D plane “Planar” and the time “Steady State”. The fluid type is selected as water, where the inlet velocity is $0.4\,m/s$ as a boundary condition. The outlet boundary condition is set to $0\ Pa$ gauge, which means the outlet is at the pre-specified atmosphere pressure. The side edges/walls have a no-slip boundary conditions so that the side walls of the water channel test section are modelled correctly. The turbine edges/walls have a no-slip boundary condition.

The most crucial part of the analysis is the “Moving Reference Frame” part, where the rotational flow field is modelled. Since the CAD geometry is created so that the origin of the wind turbine is attached to the Cartesian coordinate system origin, the center of rotation is at $x = 0\ mm$ & $y = 0\ mm$. The inner domain "Cell Zone Condition" is set to have a "Frame Motion" with a rotational velocity of $12 - 60$ rpm with $6rpm$ increments. This method enables the user to perform the analysis in steady-state conditions.

Before moving to the solving step, solution methods must be specified. For Pressure-Velocity coupling SIMPLE (Semi-Implicit Method for Pressure Linked Equations) is used. For spatial discretization, pressure and momentum are set to second order upwind. For a better convergence in the early stages of the analysis turbulent kinetic energy can be set to first order upwind. After some iterations, this option can be updated to second order upwind for better accuracy.

During the solving process, the residuals guide the user. As the default option, the solution is converged if all residuals are below $1e - 03$, but in this analysis, these convergence criteria are set to $1e - 06$. Drag and moment forces are defined to be monitored and report files are created.

Parallel computing is enabled, and higher performance in shorter simulation time is achieved. 12 cores of an “ASUS-Intel Core™ i7-4720HQ CPU @ 2.60gHz” computer are used.

3.5 Post Processing

Plotting 2D contours of velocity and pressure makes it possible to investigate blade side distributions and flow structures. The convergence can be re-checked by creating an expression, which is the net mass flow rate through the control volume/area.

3.6 Mesh Independency

To efficiently conduct a mesh independency study, primary mesh refinement parameters should be defined. In this case, the main mesh parameter is selected as the inner domain mesh size. For five different inner domain mesh sizes, five similar mesh structures with a different number of elements and nodes are generated. For all cases, the first layer thickness is chosen equal and safely as explained in the Meshing section and the inflation growth rate is 1.2 to ensure a fine inflation structure of 20 layers. To capture the precise geometry the inner domain mesh type is generated with triangular components where the curvature normal angle is $1.5\,\mathrm{deg}$ and the mesh size growth rate is 1.05. This growth occurs until the inner domain mesh reaches its predefined value shown in the first row of Table 3.2. The outer domain is meshed with quadrilateral dominant structures with a fine growth rate of 1.01.

The mesh created using the given guidelines results in the finest mesh structure of $234,434$ elements where the maximum skewness is below 0.63 and the minimum orthogonal quality is above 0.6. The average skewness and orthogonal quality values show a sufficient mesh for all five mesh structures.

The average net torque results obtained from the mesh independency study are presented in Figure 3.6. The results clearly show that Mesh-3 with roundly $91,000$ mesh elements can accurately capture the flow physics. After this point, where the inner domain mesh size equals 20 and 30 mm, the mesh structures result in a relative error larger than 10% and 16%, respectively. This clearly indicates that the mesh independency study is finalized by selecting Mesh-3 with the inner domain mesh size of 10 mm.

Table 3.2: Meshing Specifics of the study

Mesh Feature	Mesh 1	Mesh 2	Mesh 3	Mesh 4	Mesh 5
Inner Domain Mesh Size	3 mm	6 mm	10 mm	20 mm	30 mm
Inner Domain Mesh Type	Triangular	Triangular	Triangular	Triangular	Triangular
Inner Domain Growth Rate	1.05	1.05	1.05	1.05	1.05
Outer Domain Mesh Size	12 mm	24 mm	40 mm	80 mm	120 mm
Outer Domain Mesh Type	Quadrilateral D.	Quadrilateral D.	Quadrilateral D.	Quadrilateral D.	Quadrilateral D.
Outer Domain Growth Rate	1.01	1.01	1.01	1.01	1.01
First Layer Thickness	0.017 mm	0.017 mm	0.017 mm	0.017 mm	0.017 mm
Inflation Growth Rate	1.2	1.2	1.2	1.2	1.2
Number of Inflation Layers	20	20	20	20	20
Curvature Normal Angle	1,5°	1.5°	1.5°	1.5°	1.5°
Number of Elements	234 434	115 365	91 271	82 634	57 677
Number of Nodes	195 919	96 622	74 584	65 870	49 677
Average Skewness	0.066	0.055	0.051	0.046	0.044
Maximum Skewness	0.620	0.674	0.708	0.713	0.820
Average Orthogonal Q.	0.977	0.982	0.982	0.982	0.982
Minimum Orthogonal Q.	0.608	0.544	0.536	0.552	0.550

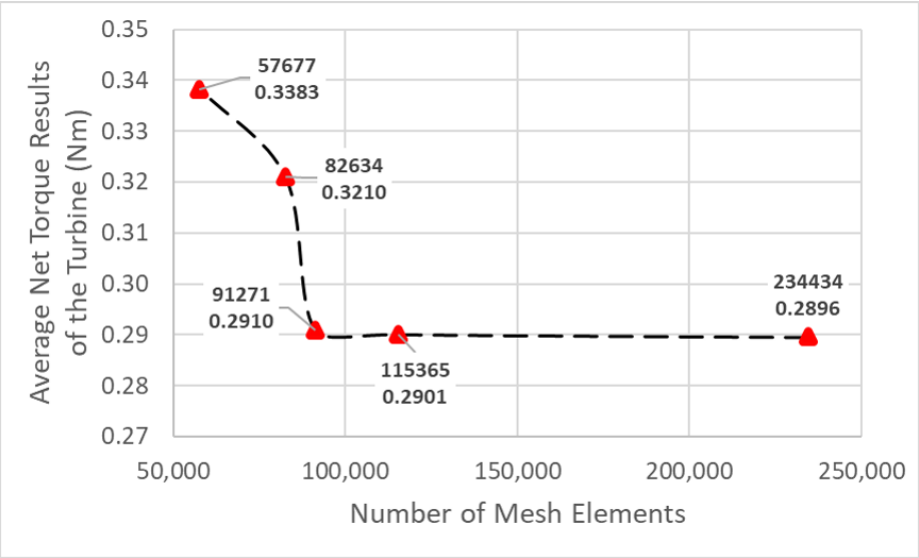

Figure 3.6: Average Net Torque Results for the five meshes of the independency study

CHAPTER 4

EXPERIMENTAL AND COMPUTATIONAL RESULTS

For the inflow velocity condition of $0.40\ m/s$, the three base geometries selected are investigated in both experimental and computational studies. The monitored output parameters where rotational velocity (or angular position converted into rotational velocity) and torque of the Savonius turbine. The rated values of these are converted to non-dimensional parameters tip speed ratio, power and torque coefficient, using Equations 1.6, 1.5, and 1.10, respectively.

There is a consistency throughout this chapter, were results of Base Geometry 1, 2, and 3 are presented in blue ($\triangle$), orange ($\bigcirc$), and green ($\square$). While experimental results are shown in solid lines, CFD results are plotted in dashed lines.

4.1 Experimental Results

Considering the $0 - 60\ rpm$ range with $6\ rpm$ increments for an inflow of $0.4\ m/s$ results in a tip speed ratio variation from 0 to roundly 2.5. For each base geometry, eleven data points are recorded and performance parameters are plotted against the tip speed ratio. Figure 4.1 illustrates the power coefficient of the base geometries. The inverted U-shape performance curve is characteristic of Savonius turbines and this trend is clearly seen in all experimental results. Since rotational velocity is a multiplier of C_P, at low tip speed ratio values (between $0 - 0.75$) the power coefficient is relatively small but experiences a monotonic increase with increasing λ. At around $0.95 - 1.5$ tip speed ratio values, the turbines of interest experience a peak in performance. After this peak, although rotational velocity increases, another multiplier decreases to finalize the inverted U-shape. With decreasing torque values measured,

the trend monotonically decreases and even results in negative C_P values. This can be interpreted as a change in turbomachinery characteristics. Up to a tip speed ratio the Savonius turbine inside the water channel extracts energy and is categorized as energy producing device. After this point, the torque values further decrease and the motor attached to the turbine shaft begins to supply the necessary torque for the constant angular speed movement. Thus the turbine is consuming energy and results in negative power coefficient values.

Experimental results of Figure 4.1 show that for positive C_P values, Base Geometry 2 power coefficient values are approximately half of the Base Geometry 1 results. The maximum power coefficient is around unity tip speed ratio and is less than 0.2. The positive characteristic for the Base Geometry 2 turbine is recorded and calculated to be between $0 - 1.75$.

Base Geometry 1 and 3 are similar in results up to a 1.75 tip speed ratio, where maximum C_P values are calculated as 0.35 and 0.33, respectively. Both peak around $1 - 1.5$ tip speed, but Base Geometry 3 has a larger positive performance curve interval. For $\lambda > 2$, while Base Geometry 1 experiences a negative power coefficient, Base Geometry 3 has a C_P equal to 0.1.

To understand the self-starting ability of the Savonius turbines, another performance parameter, torque coefficient is calculated and plotted against tip speed ratio in Figure 4.2. After a 0.5 tip speed ratio, a monotonic decrease in torque coefficient is seen for all base geometries. Base Geometry 3 experiences the highest C_Q values with nearly 0.5.

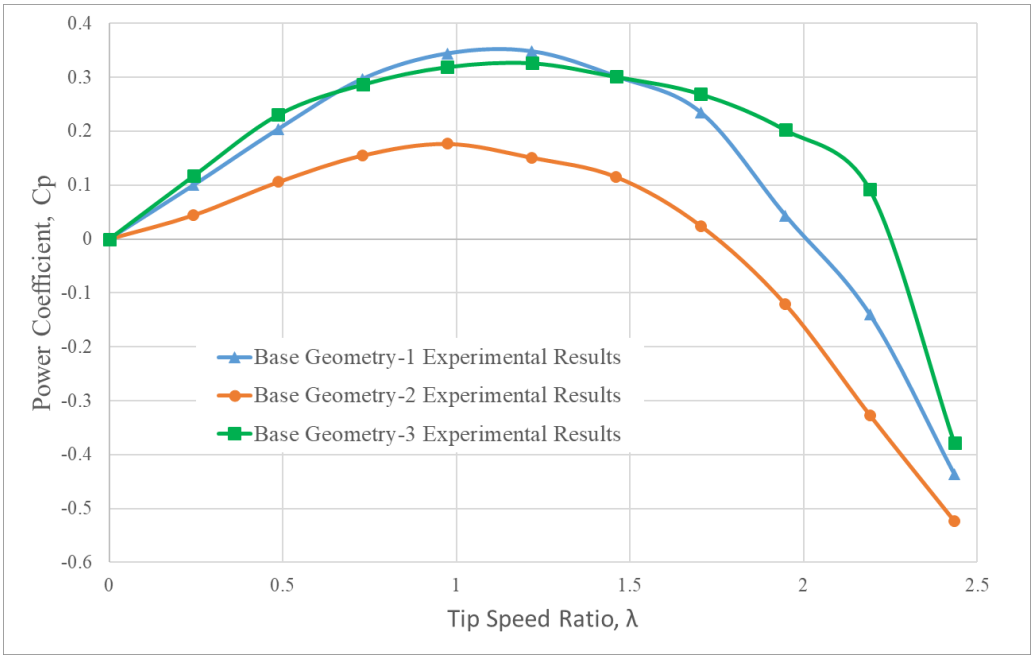

Figure 4.1: Experimental results of power coefficient, C_P versus tip speed ratio, λ for the 3 base geometries

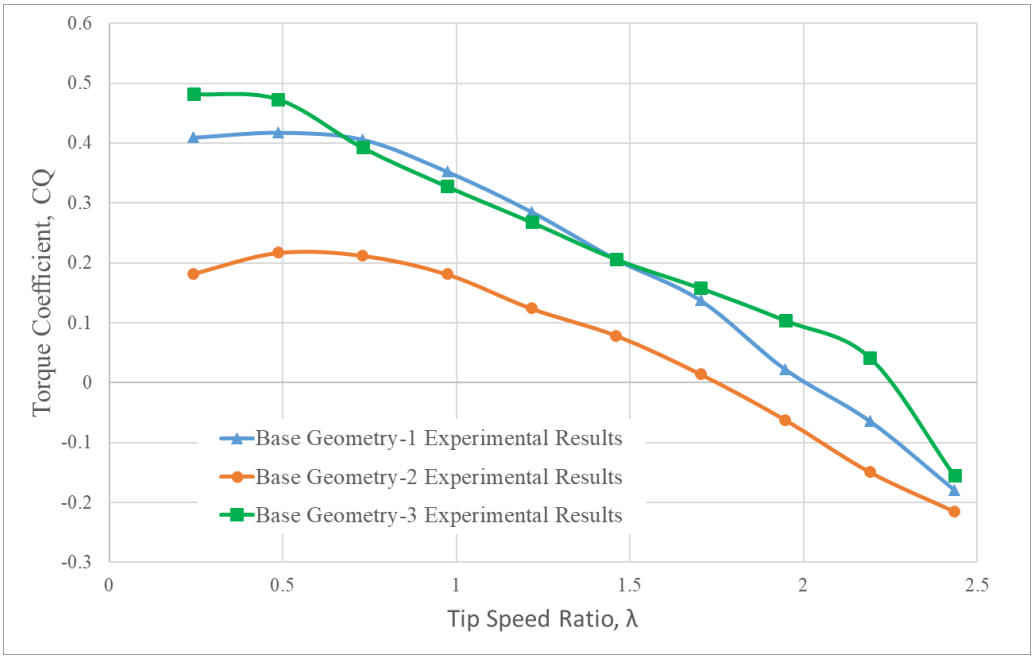

Figure 4.2: Experimental results of torque coefficient, C_Q versus tip speed ratio, λ for the 3 base geometries

4.2 Computational Results

Using the converged torque results of computational studies, Figures 4.3 and 4.4 are created. The positive to negative performance characteristics change is experienced by all turbines in this study.

While Base Geometry 1 and 2 experience similar trends, where the inverted U-shape can be clearly distinguished, Base Geometry 3 results show a trend where the performance peaks at a higher tip speed ratio. Both Base Geometry 1 and 3 peak to a power coefficient of roundly 0.32. However, while Base Geometry 1 experiences this peak at roundly unity tip speed ratio, Base Geometry 3 achieves this result at twice this tip speed. According to the CFD results shown in Figure 4.4, Base Geometry 1 has the best self-starting ability for $\lambda > 1.5$ and has a maximum where $C_Q = 0.37$.

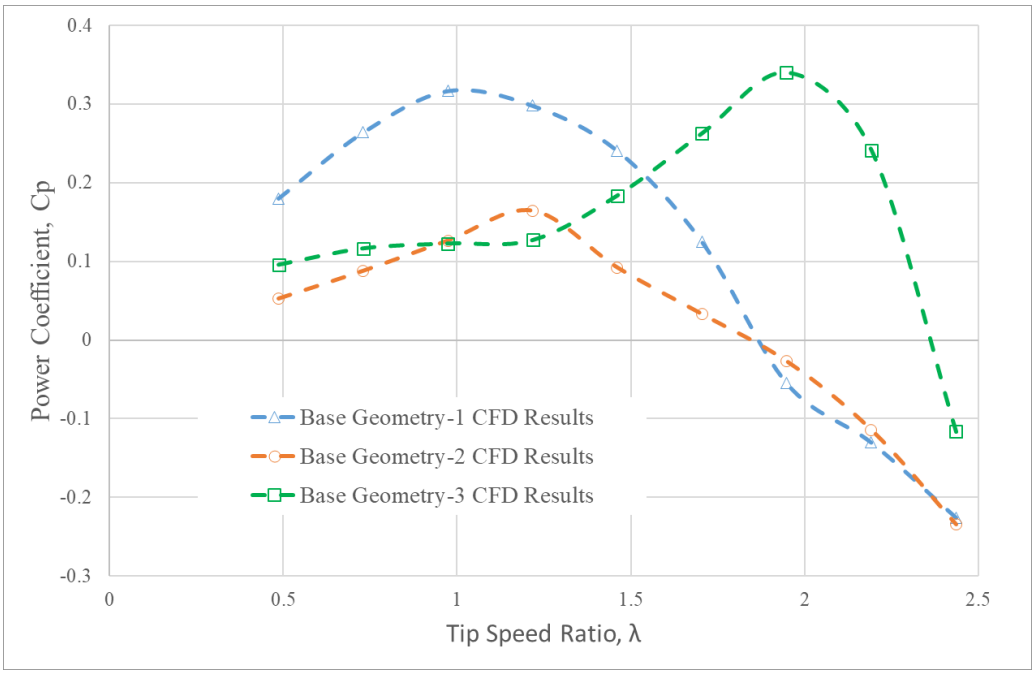

Figure 4.3: Computational results of power coefficient, C_P versus tip speed ratio, λ for the 3 base geometries

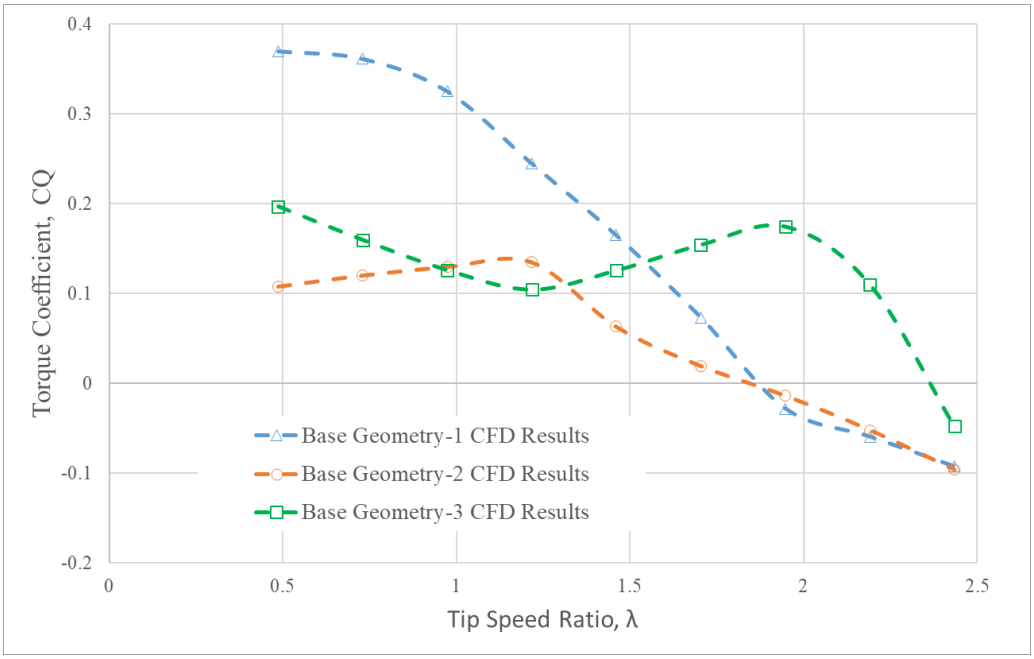

Figure 4.4: Computational results of torque coefficient, C_Q versus tip speed ratio, λ for the 3 base geometries

4.3 Comparison of Experimental and Computational Results

4.3.1 Base Geometry 1: Semi-circular Shape

Figure 4.5 shows a good agreement in experimental and computational values where both peak around unity tip speed ratio and for maximum power coefficient the relative error is 7.8%. For $\lambda < 2$ where all C_P values are positive, computational results underestimate the performance compared to experimental results. While for smaller tip speeds power coefficient results deviate less than 0.03, with increasing tip speed this deviation reaches up to 0.1.

Comparing the torque coefficient results, Figure 4.6 illustrates the similarity in experimental and computational results. The relative error for small tip speed ratios is less than 15%.

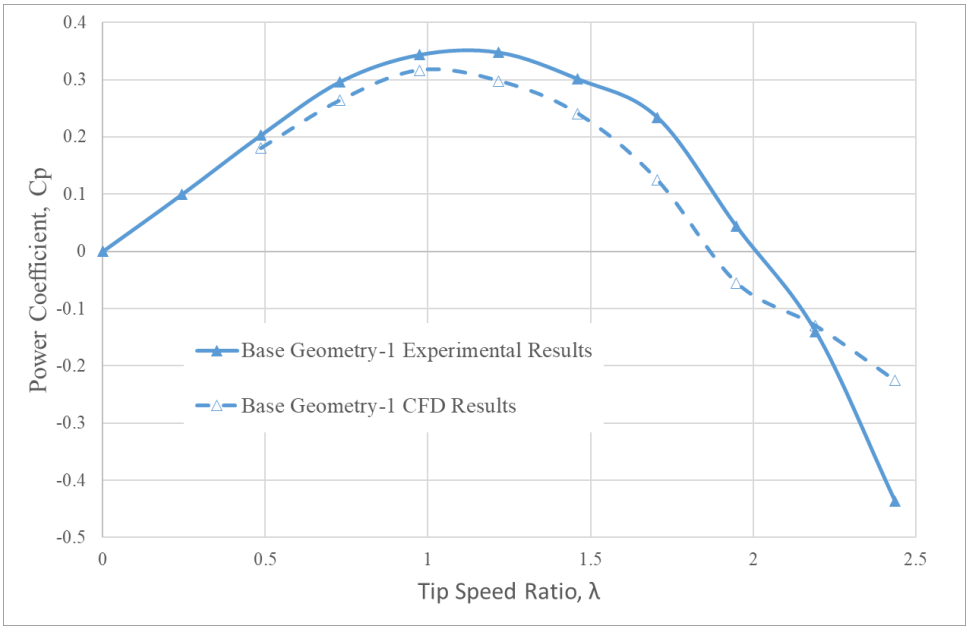

Figure 4.5: Experimental and computational results of power coefficient, C_P versus tip speed ratio, λ for Base Geometry 1

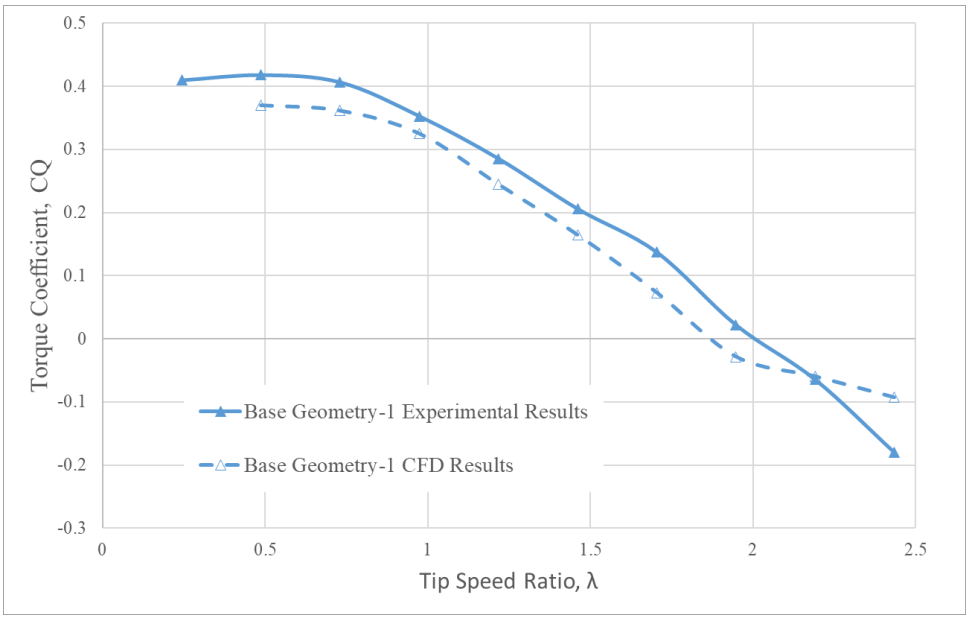

Figure 4.6: Experimental and computational results of torque coefficient, C_Q versus tip speed ratio, λ for Base Geometry 1

4.3.2 Base Geometry 2: Liskiewicz's Elliptical Shape

Figure 4.7 shows that both experimental and computational results result in a performance curve with a distinct inverted U-shape. For small and large tip speed values of the spectrum the error increases between the experimental and computational studies. For a tip speed ratio range of roundly $1.1 - 1.7$ the results are in a good numeric agreement with a deviation of not larger than 0.025. While computational studies predict the maximum C_P at $\lambda = 1.22$, experiments peak at $\lambda = 0.97$.

The same agreement accuracy can be seen in Figure 4.8, where for tip speed ratios less than unity, experimental results are predict a larger C_Q value around 0.22 and computations predict torque coefficients less than 0.14.

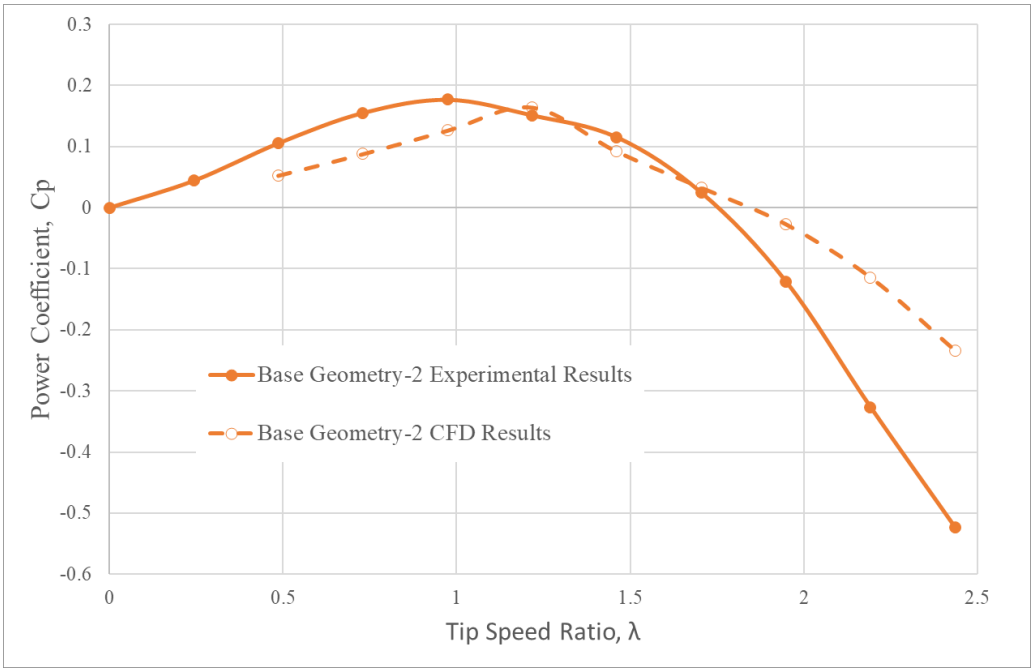

Figure 4.7: Experimental and computational results of power coefficient, C_P versus tip speed ratio, λ for Base Geometry 2

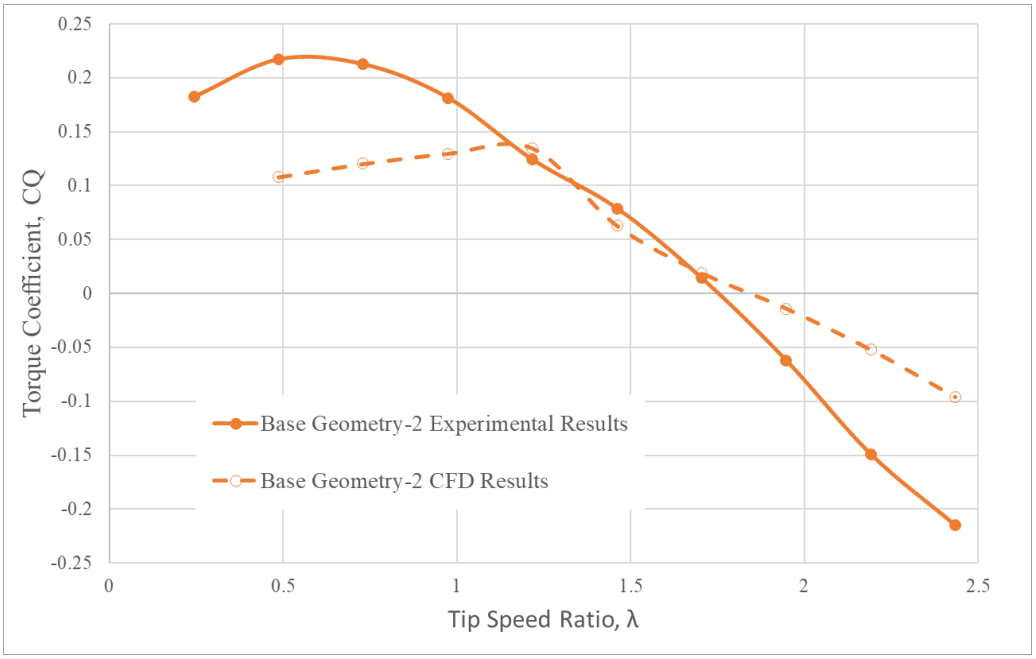

Figure 4.8: Experimental and computational results of torque coefficient, C_Q versus tip speed ratio, λ for Base Geometry 2

4.3.3 Base Geometry 3: Saha's Elliptical Shape

Figure 4.9 gives a basis for the comparison of Base Geometry 3. Experimental results follow the inverted U-shaped trend with the largest interval of positive performance of all base geometries. The computational studies predict a behaviour of nearly constant power coefficient up to 1.2 tip speed and an inverted U-shape afterwards. This results in a mismatch in peak performance tip speed between experimental and computational studies. Experimental results experience a power coefficient result greater than 0.3 in a tip speed ratio interval of $0.7 - 1.5$, while computational studies predict this interval to be $1.8 - 2.1$.

The high torque values calculated in CFD for larger angular velocities influenced the torque coefficient results too, where Figure 4.10 clearly illustrates this situation. While experimental results predicts a torque coefficient near 0.5, computational studies calculated the maximum torque coefficient as 0.2.

Figure 4.9: Experimental and computational results of power coefficient, C_P versus tip speed ratio, λ for Base Geometry 3

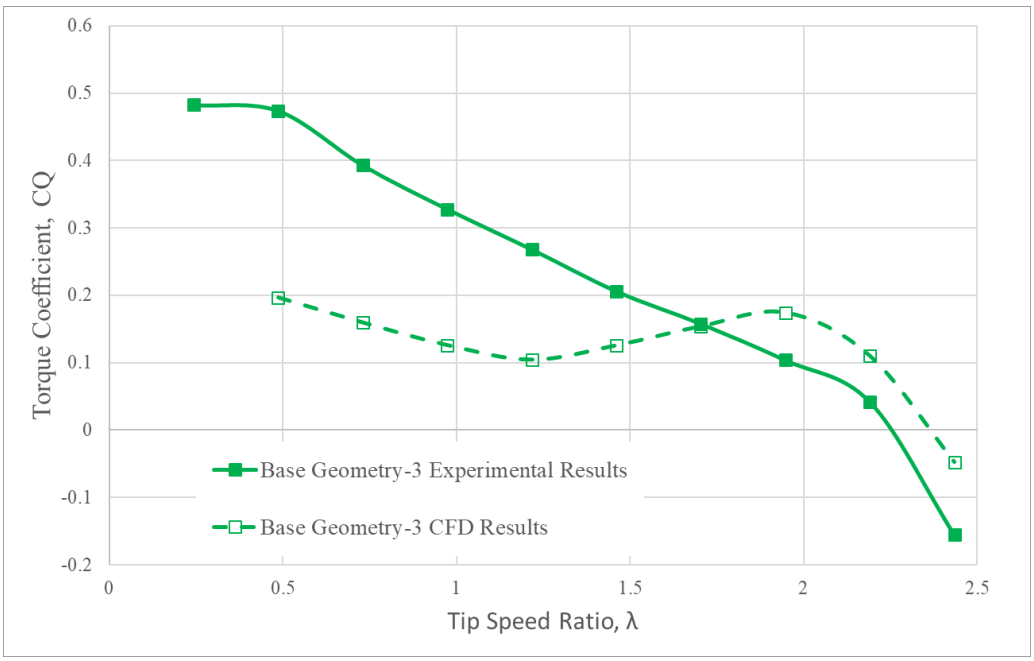

Figure 4.10: Experimental and computational results of torque coefficient, C_Q versus tip speed ratio, λ for Base Geometry 3

CHAPTER 5

CONCLUSION

The main goal of this thesis study is to create, i.e. set up, the crucial capabilities to design a drag-based cross-flow hydrokinetic turbine. The experimental and computational studies created the foundation of this thesis.

Three base geometries are selected from the literature and investigated for a discrete water channel/inflow velocity value. Rotational velocity, thus tip speed ratio, is controlled by a motor and torque results are monitored and mathematically converted to non-dimensional performance parameters.

Using commercial ANSYS software, a mesh indecency study is conducted and the optimal mesh number is determined. Using this mesh, base geometries are analyzed inside the Fluent Solver and important parameters are monitored and stored.

Considering limited computational power, a 2D computational study is conducted. This introduced a challenge where the 3D effects of a Savonius turbine should be minimized so that a reasonable comparison can be made. Three elements are taken into account so that 3D effects would not dominate the experimental procedure:

- Not having a twist angle in the Savonius Turbine or not having any separate vertical sections.
- Having a H/D ratio greater or equal to 1, where 3D effects are minimized [5] (though the 3D effects are not totally eliminated)
- Using end plates to eliminate the pressure contour in the height direction, at the top and bottom of the turbine.

The conclusions of this thesis study can be as such:

- Using an computational outer domain with the same dimensions as the experimental study domain resulted in more reliable comparison between results. The same domain sizes of computational and experimental studies made it possible to compare the results while the blockage ratio is 18.5%. To find the corrected Savonius turbine performance, a blockage correction can be applied.

- Although having an aspect ratio of unity is discussed to be the acceptable minimum, it could effect the results. The influence of the aspect ratio can be investigated in further studies.

- Both experimental and computational performance curve trends are in good agreement with the literature, where an inverted U-shape can be seen for all power coefficient results and calculations.

- Experimental power coefficient results show that Base Geometry 1 and 3 are similar up to a 1.75 tip speed ratio, where maximum C_P values are found as 0.35 and 0.33, respectively. The main difference between these turbines is that the Base Geometry 3 produces more energy at higher tip speed ratios and for a larger tip speed interval than Base Geometry 1.

- The "Moving Reference Frame" approach resulted in reliable results to compare to experimental studies. This approach can be further improved by implementing Fluent's 6-DOF capabilities.

- Base Geometry 1 (perfect semi-circular blade shape) has the best validation of experimental and computational studies where both peak around unity tip speed ratio. The relative error of the maximum power coefficient found to be 7.8%.

- Compared to a perfect semi-circular shape (Base Geometry 1) a blade with a maximum chamber location near the tip (Base Geometry 2) resulted in smaller torque, i.e. power and torque coefficient, values. By moving the maximum chamber location near the tip the negative torque of the returning blade could be maximized, thus net torque produced is reduced. Further investigation can be performed to find the optimal maximum chamber location.

- Base Geometry 3 (smaller chamber than Base Geometry 1 and 2) experimental and computational results deviated considerably. Although the general trend is an inverted U-shape in both studies, the numeric values of peak performance tip speed ratios are different.

Although 3D effects aimed to be minimized (not having a twist angle, AR = 1, and using end plates) the deviation of results could be further investigated by studies focused on the aspect ratio.

The detailed explanation and built capabilities explained in this thesis, forms the foundation of many experimental studies that are planned to be conducted in the water channel. This study only includes the calibration of the channel and an investigation of the Savonius Water Turbine. Though, the future work can be much more exclusive, covering the investigation of flow structures using advanced measurement techniques such as PIV, study of 3D effects of Savonius type VAWTs (helix angle), study of Darrieus type VAWTs and hydrokinetic turbines, study of combined (Savonius + Darrieus) turbines, sensitivity analysis of geometric design parameters (D/H ratio, end plate ratio, overlap ratio, etc.), study of partially submerged VAWTs and many more.

Measuring the flow field using PIV and investigating 3D effects of the Savonius turbine can be crucial step for the future studies. Interpreting the flow field in full detail can be the key to understand the difference between computational and experimental results. The investigation of three-dimensional effects can address the difference in results found in this thesis.

REFERENCES

[1] M. J. Alam and M. T. Iqbal, "Design and development of hybrid vertical axis turbine," in *2009 Canadian conference on electrical and computer engineering*, pp. 1178–1183, IEEE, 2009.

[2] G. Saini and R. P. Saini, "A review on technology, configurations, and performance of cross-flow hydrokinetic turbines," *International Journal of Energy Research*, vol. 43, no. 13, pp. 6639–6679, 2019.

[3] C. Ma, L. Song, and M.-Z. Zhang, "Performance study for a novel vertical axis wind turbine based on simulation analysis," in *2017 IEEE 14th International Conference on Networking, Sensing and Control (ICNSC)*, pp. 549–554, 2017.

[4] K. Kacprzak, G. Liskiewicz, and K. Sobczak, "Numerical investigation of conventional and modified savonius wind turbines," *Renewable energy*, vol. 60, pp. 578–585, 2013.

[5] P. K. Talukdar, A. Sardar, V. Kulkarni, and U. K. Saha, "Parametric analysis of model savonius hydrokinetic turbines through experimental and computational investigations," *Energy Conversion and Management*, vol. 158, pp. 36–49, 2018.

[6] T. M. Letcher, *Wind energy engineering: A handbook for onshore and offshore wind turbines*. Academic Press, 2017.

[7] "Frequently Asked Questions (FAQs) - U.S. Energy Information Administration (EIA)," jul 28 2022. [Online; accessed 2022-07-30].

[8] "2022 Hydropower Status Report," dec 20 2021. [Online; accessed 2022-07-30].

[9] M. M. Kamal and R. Saini, "A review on modifications and performance assessment techniques in cross-flow hydrokinetic system," *Sustainable Energy Technologies and Assessments*, vol. 51, p. 101933, 2022.

[10] Y. Chu, Y. Pan, H. Zhan, W. Cheng, L. Huang, Z. Wu, and L. Shao, "Systems accounting for carbon emissions by hydropower plant," *Sustainability*, vol. 14, no. 11, p. 6939, 2022.

[11] M. Sood and S. K. Singal, "Development of hydrokinetic energy technology: A review," *International Journal of Energy Research*, vol. 43, no. 11, pp. 5552–5571, 2019.

[12] E. Quaranta, A. Bahreini, A. Riasi, and R. Revelli, "The very low head turbine for hydropower generation in existing hydraulic infrastructures: State of the art and future challenges," *Sustainable Energy Technologies and Assessments*, vol. 51, p. 101924, 2022.

[13] J. V. Akwa, H. A. Vielmo, and A. P. Petry, "A review on the performance of savonius wind turbines," *Renewable and sustainable energy reviews*, vol. 16, no. 5, pp. 3054–3064, 2012.

[14] G. Saini and R. Saini, "A computational investigation to analyze the effects of different rotor parameters on hybrid hydrokinetic turbine performance," *Ocean Engineering*, vol. 199, p. 107019, 2020.

[15] A. Bahaj and L. E. Myers, "Fundamentals applicable to the utilisation of marine current turbines for energy production," *Renewable energy*, vol. 28, no. 14, pp. 2205–2211, 2003.

[16] S. Savonius, "Rotor adapted to be driven by wind or flowing water," Jan. 1 1929. US1697574A.

[17] A. S. Saad, I. I. El-Sharkawy, S. Ookawara, and M. Ahmed, "Performance enhancement of twisted-bladed savonius vertical axis wind turbines," *Energy Conversion and Management*, vol. 209, p. 112673, 2020.

[18] A. Damak, Z. Driss, and M. Abid, "Experimental investigation of helical savonius rotor with a twist of 180," *Renewable Energy*, vol. 52, pp. 136–142, 2013.

[19] I. Ross and A. Altman, "Wind tunnel blockage corrections: Review and application to savonius vertical-axis wind turbines," *Journal of Wind Engineering and Industrial Aerodynamics*, vol. 99, no. 5, pp. 523–538, 2011.

[20] B. F. Blackwell, L. V. Feltz, and R. E. Sheldahl, *Wind tunnel performance data for two-and three-bucket Savonius rotors*. Sandia Laboratories Springfield, VA, USA, 1977.

[21] M. Mohamed, G. Janiga, E. Pap, and D. Thévenin, "Optimization of savonius turbines using an obstacle shielding the returning blade," *Renewable Energy*, vol. 35, no. 11, pp. 2618–2626, 2010.

[22] U. Saha, S. Thotla, and D. Maity, "Optimum design configuration of savonius rotor through wind tunnel experiments," *Journal of Wind Engineering and Industrial Aerodynamics*, vol. 96, no. 8-9, pp. 1359–1375, 2008.

[23] W. El-Askary, A. S. Saad, A. M. AbdelSalam, and I. Sakr, "Investigating the performance of a twisted modified savonius rotor," *Journal of Wind Engineering and Industrial Aerodynamics*, vol. 182, pp. 344–355, 2018.

[24] M. Tartuferi, V. D'Alessandro, S. Montelpare, and R. Ricci, "Enhancement of savonius wind rotor aerodynamic performance: a computational study of new blade shapes and curtain systems," *Energy*, vol. 79, pp. 371–384, 2015.

[25] V. Patel, G. Bhat, T. Eldho, and S. Prabhu, "Influence of overlap ratio and aspect ratio on the performance of savonius hydrokinetic turbine," *International Journal of Energy Research*, vol. 41, no. 6, pp. 829–844, 2017.

[26] J. Thiyagaraj, I. Rahamathullah, R. Bharathiraja, G. Anbuchezhiyan, and A. Ponshanmugakumar, "Influence of various augmentation devices on the performance characteristics of modified four bladed fixed flip type savonius hydrokinetic turbine," *Materials Today: Proceedings*, vol. 46, pp. 3665–3669, 2021.

[27] A. H. Birjandi, E. L. Bibeau, V. Chatoorgoon, and A. Kumar, "Power measurement of hydrokinetic turbines with free-surface and blockage effect," *Ocean Engineering*, vol. 69, pp. 9–17, 2013.

[28] C. Lartiga and C. Crawford, "Water tunnel rotor testing with post processing based on piv measurements," in *ASME International Mechanical Engineering Congress and Exposition*, vol. 44298, pp. 1087–1095, 2010.

[29] N. Fujisawa, “On the torque mechanism of savonius rotors,” *Journal of Wind Engineering and Industrial Aerodynamics*, vol. 40, no. 3, pp. 277–292, 1992.

[30] M. Tahani, A. Rabbani, A. Kasaeian, M. Mehrpooya, and M. Mirhosseini, “Design and numerical investigation of savonius wind turbine with discharge flow directing capability,” *Energy*, vol. 130, pp. 327–338, 2017.

[31] H. Aksel, M. M. Yavuz, and E. Demircan, “Bap – 2 teknolojik araştırma projeleri raporu - değişik kanat profillerinin darrieus tipi su türbinlerinin performansına etkisinin deneysel olarak incelenmesi,” 2013.